Mitochondrial Targeting of the Ammonia-Sensitive Uncoupler SLC4A11 by the Chaperone-Mediated Carrier Pathway in Corneal Endothelium

Moonjung Choi and Joseph A. Bonanno

Vision Science Program, Indiana University, School of Optometry, Bloomington, Indiana, United States

Correspondence: Joseph A. Bonanno, Vision Science Program, School of Optometry, Indiana University, Bloomington, IN 47405, USA;
jbonanno@indiana.edu.

Received: June 10, 2021
Accepted: August 11, 2021
Published: September 9, 2021

Citation: Choi M, Bonanno JA. Mitochondrial targeting of the ammonia-sensitive uncoupler SLC4A11 by the chaperone-mediated carrier pathway in corneal endothelium. *Invest Ophthalmol Vis Sci.* 2021;62(12):4.
https://doi.org/10.1167/iovs.62.12.4

Purpose. SLC4A11, an electrogenic H^+ transporter, is found in the plasma membrane and mitochondria of corneal endothelium. However, the underlying mechanism of SLC4A11 targeting to mitochondria is unknown.

Methods. The presence of mitochondrial targeting sequences was examined using in silico mitochondrial proteomic analyses. Thiol crosslinked peptide binding to SLC4A11 was screened by untargeted liquid chromatography/tandem mass spectrometry (LC-MS/MS) analysis. Direct protein interactions between SLC4A11 and chaperones were examined using coimmunoprecipitation analysis and proximity ligation assay. Knockdown or pharmacologic inhibition of chaperones in human corneal endothelial cells (HCECs) or mouse corneal endothelial cells (MCECs), ex vivo kidney, or HA-SLC4A11–transfected fibroblasts was performed to investigate the functional consequences of interfering with mitochondrial SLC4A11 trafficking.

Results. SLC4A11 does not contain canonical N-terminal mitochondrial targeting sequences. LC-MS/MS analysis showed that HSC70 and/or HSP90 are bound to HA-SLC4A11–transfected PS120 fibroblast whole-cell lysates or isolated mitochondria, suggesting trafficking through the chaperone-mediated carrier pathway. SLC4A11 and either HSP90 or HSC70 complexes are directly bound to the mitochondrial surface receptor, TOM70. Interference with this trafficking leads to dysfunctional mitochondrial glutamine catabolism and increased reactive oxygen species production. In addition, glutamine (Gln) use upregulated SLC4A11, HSP70, and HSP90 expression in whole-cell lysates or purified mitochondria of HCECs and HA-SLC4A11–transfected fibroblasts.

Conclusions. HSP90 and HSC70 are critical in mediating mitochondrial SLC4A11 translocation in corneal endothelial cells and kidney. Gln promotes SLC4A11 import to the mitochondria, and the continuous oxidative stress derived from Gln catabolism induced HSP70 and HSP90, protecting cells against oxidative stress.

Keywords: mitochondrial protein import, HSP90, HSC70, cornea, kidney, oxidative stress

SLC4A11, a member of the SLC4 family of bicarbonate transporters, codes an ~100-kDa protein with 14 transmembrane domains that assembles in plasma membranes as dimers.[1–3] Although first thought to be a bicarbonate transporter and then a borate transporter, it is now known to function as an NH_3-sensitive electrogenic H^+ transporter.[1,4–6] SLC4A11 is ubiquitously expressed in mammalian tissues with prominent expression in duodenum, colon, pancreas, ovary, kidney, cochlea, and cornea.[7] Homozygous recessive mutations in *SLC4A11* cause congenital hereditary endothelial dystrophy (CHED), which is manifested as poor vision due to corneal edema secondary to dysfunctional corneal endothelial (CE) cells and called Harboyan syndrome when associated with hearing deficits.[3,8,9] *Slc4a11* knockout (KO) mice recapitulate the features of CHED with progressive corneal edema at eye opening, concurrent oxidative stress, gradual loss of CE, and hearing and renal deficits.[10,11] Whereas SLC4A11 is clearly targeted to the plasma membrane, multiple cytoplasmic locations have been documented[12,13] and most recently confirmed to be an inner mitochondrial membrane (IMM) protein.[14] Whereas SLC4A11 expression is ubiquitous, only cornea and hearing deficits have been reported in humans with mutations. This may be due to lack of study of the rare homozygous defects, less important glutamine catabolism, or other compensatory pathways not present in the corneal endothelium.

In mitochondria, glutaminase catalyzes the conversion of glutamine (Gln) to glutamate (Glu). Glu can be converted to α-ketoglutarate (α-KG) via glutamate dehydrogenase. This step reduces NADP to NADPH. Both steps produce a molecule of NH_3 and α-KG can enter the tricarboxylic acid (TCA) cycle. Gln oxidation correlates with increased reactive oxygen species (ROS) production by its stimulation of the electron transport chain (ETC).[15–17] As such, the NH_3-sensitive properties of SLC4A11 are ideal for the higher pH mitochondrial environment, where it restrains IMM hyperpolarization during Gln catabolism.[14] Absence of SLC4A11 in

Copyright 2021 The Authors

This work is licensed under a Creative Commons Attribution-NonCommercial-NoDerivatives 4.0 International License.

the mitochondria leads to excess mitochondrial ROS, mitochondrial disruption, and apoptosis that could be rescued by pharmacologic mitochondrial uncoupling or bypassing glutamine catabolism.[14] These results and previous studies showing multiple cytoplasmic locations[12,13,18] indicate a complex pattern of SLC4A11 trafficking. However, the underlying mechanism by which SLC4A11 trafficks to the IMM has not been investigated.

Nucleus-encoded mitochondrial precursor proteins are imported to mitochondria passing through the translocase of the outer membrane (TOM) complex by two general sorting mechanisms: (1) canonical mitochondrial-targeting signals at the N-terminus of the protein (aka the presequence pathway) or (2) discontinuous cryptic targeting signals spread throughout the protein (aka the carrier pathway).[19] In contrast to presequence trafficking, carrier-mediated import requires association with molecular chaperones in the cytosol (e.g., heat shock proteins; HSP90, HSP70, and/or HSC70) and in the mitochondrial intermembrane space (e.g., TIM9–TIM10 and homologous TIM8–TIM13) to prevent aggregation and to guide the proteins to their destination in the mitochondria.[19–22] In particular, cytosolic chaperones deliver their cargo specifically to the mitochondrial surface receptor TOM70.[21,23,24] Lack of mitochondrial targeting presequences indicates that a carrier-mediated mechanism is likely.[19,25]

In the current study, we explore mitochondrial SLC4A11 import using in silico mitochondrial proteomic analyses and chemical crosslinking coupled with mass spectrometry analysis, which suggests that SLC4A11 trafficking into the IMM uses the chaperone-mediated carrier pathway. Blocking SLC4A11 translocation to mitochondria by either inhibition or knockdown of the chaperone HSP90 or HSC70 dampens Gln-dependent proton leak–linked mitochondrial respiration and accelerates mitochondrial ROS production, highlighting the major determinant of cytosolic chaperones in mitochondrial SLC4A11 trafficking. Interestingly, Gln enhances HSP70 and HSP90 expression and increased mitochondrial SLC4A11 import, which in turn guards against excess oxidative stress during Gln catabolism. Furthermore, mitochondrial distribution of Slc4a11 and its trafficking mediated via HSP90 are also observed in the kidney. Overall, our results reveal that recruitment of SLC4A11 by the chaperone complex of HSP90 or HSC70 in the cytoplasm is a crucial step in the initiation of mitochondrial SLC4A11 trafficking to the IMM.

Methods

Mice

Slc4a11 KO mice[10] were housed and maintained in pathogen-free conditions and used in the experiments in compliance with institutional guidelines and the current regulations of the National Institutes of Health, the US Department of Health and Human Services, the US Department of Agriculture, and the ARVO Statement for the Use of Animals in Ophthalmic and Vision Research.

Cell Culture

Conditionally immortalized mouse corneal endothelial cell (MCEC) *Slc4a11* wild-type (WT) and knockout (KO)[26] were cultured in an OptiMEM-I medium (#51985; Thermo Fisher Scientific, Canoga Park, CA, USA) supplemented with 8% heat-inactivated fetal bovine serum (#10082139; Thermo Fisher Scientific), 5 ng/mL EGF (#01-107; Millipore, Darmstadt, Germany), 100 µg/mL pituitary extract (Hyclone Laboratories, Logan, UT, USA), 0.08% chondroitin sulfate (#G6737; Sigma-Aldrich, St. Louis, MO, USA), 200 mg/L calcium chloride, 1% antibiotic/antimycotic solution (#15240062; Thermo Fisher Scientific), 50 µg/mL gentamicin (#15710072; Thermo Fisher Scientific), and 44 U/mL IFN-γ (#485-MI; R&D Systems, Minneapolis, MN, USA) at 33°C. Immortalized human corneal endothelial cells (HCECs)[27] were maintained in the same medium as the MCECs but not supplemented with IFN-γ at 37°C. Stable transfection of human SLC4A11-HA tagged (hSLC4A11-HA) or empty vector (EV) into the PS120 Chinese hamster CCL39 fibroblast cell line was generated as described previously[4] and cultured in DMEM (#21063; Thermo Fisher Scientific), supplemented with 5% heat-inactivated fetal bovine serum (FBS; #10082139; Thermo Fisher Scientific), 1 mg/mL Geneticin (#10131027; Thermo Fisher Scientific), and 1% antibiotic/antimycotic (#15240062; Thermo Fisher Scientific) at 37°C. All cultures were grown under 5% CO_2 in a humidified incubator and replaced with fresh medium every other day.

In Silico Analysis

The presence of N-terminal mitochondrial targeting sequences was predicted with four widely used software tools: MitoProt II (https://ihg.gsf.de/ihg/mitoprot.html),[28,29] TargetP 2.0 (http://www.cbs.dtu.dk/services/TargetP/),[30] iPSORT (http://www.hypothesiscreator.net/iPSORT/),[31] and Predotar (https://urgi.versailles.inra.fr/predotar/).[32] A rule-based algorithm used several common properties of the N-terminal mitochondrial presequence, such as the composition of at least two positively charged particular amino acid residues, the absence of acidic residues in a targeting sequence, the existence of a cleavage site, and the capacity of forming α-helical amphiphilic structures in the N-terminal region.

Mitochondrial Purification From the Cultured Cells

The cell pellet was prepared as described previously.[14] Briefly, cells were ruptured with prechilled glass Dounce homogenizer, followed by centrifugation at 1000 × *g* for 10 minutes at 4°C. The supernatant was collected into new tubes, and the pellet containing unbroken cells and nuclei was discarded. The supernatant was centrifuged at 12,000 × *g* for 15 minutes at 4°C. The pellet containing mitochondria was washed with ice-cold isotonic mitochondrial buffer (IB-2; 10 mM Tris-MOPS, 200 mM sucrose, pH 7.4) supplemented with complete protease inhibitor cocktail (#11697498001; Roche, Basel, Switzerland) and centrifuged at 12,000 × *g* for 10 minutes at 4°C, and this washing step was repeated twice. The intact mitochondria in the pellet were collected into IB-2. The supernatant, containing mostly cytoplasmic and plasma membrane proteins, was saved as a cytosolic fraction indicator. The protein concentrations of resuspended mitochondria were quantified using a BCA assay (#23225; Thermo Fisher Scientific).

DSP Crosslinking Coupled With Liquid Chromatography/Tandem Mass Spectrometry

For whole-cell crosslinking, cells were washed with prechilled PBS twice and incubated in PBS containing 2 mM

Investigative Ophthalmology & Visual Science

dithiobis (succinimidyl propionate) (DSP) (#22586; Thermo Fisher Scientific), a membrane-permeant crosslinker, at 4°C for 30 minutes. For isolated mitochondria crosslinking, mitochondrial pellets were incubated in 2 mM DSP in isotonic mitochondrial buffer (IB-2; 10 mM Tris-MOPS, 200 mM sucrose, pH 7.4) at 4°C for 30 minutes. To stop crosslinking reactions, the cells/mitochondria were incubated with quenching buffer (20 mM Tris, pH 7.5) at 4°C for 15 minutes. Then, cells/mitochondria were rinsed with PBS twice and then lysed in RIPA buffer (#9806; Cell Signaling Technology, Danvers, MA, USA) with addition of 1 mM phenylmethanesulfonyl fluoride (PMSF) (#8553; Cell Signaling Technology).

SLC4A11 and associated proteins in an equal volume of lysates (from whole cells or isolated mitochondria) were immunoprecipitated by incubation with an anti-HA antibody (#901501; BioLegend, San Diego, CA, USA). Proteins were eluted from the beads with 4 M urea in 25 mM NH_4HCO_3 at 100°C for 7 minutes and then collected, followed by centrifugation at 16,000 × *g* for 15 minutes. Samples were incubated for 45 minutes at 57°C with 10 mM Tris(2-carboxyethyl)phosphine hydrochloride to reduce cysteine residue side chains. These side chains were then alkylated with 20 mM iodoacetamide for 1 hour in the dark at 21°C. Aliquots (40 µg protein) were taken and diluted to 1 M urea using 100 mM NH_4HCO_3. Trypsin was added at 1:100 w/w, and the samples were digested for 14 hours at 37°C. Individual samples were desalted using ZipTip pipette tips (EMD Millipore, Burlington, MA, USA), dried down, and resuspended in 0.1% formic acid. Fractions were analyzed by liquid chromatography/mass spectrometry (LC-MS) on an Orbitrap Fusion Lumos equipped with an Easy NanoLC1200 (Thermo Scientific, Canoga Park, CA, USA). Peptides were fragmented by high-energy collisional dissociation. Precursor ions were measured in the Orbitrap with a resolution of 120,000. Fragment ions were measured in the Orbitrap with a resolution of 60,000.

For the MS data analysis, Protein Prospector V 5.22.1 (https://prospector.ucsf.edu/prospector/mshome.htm) was used to quantify the relative amounts in a label-free quantification manner. Data were searched against the *Cricetulus griseus* proteome downloaded from Uniprot on July 12, 2017. Trypsin was set as the protease with up to two missed cleavages allowed. Oxidation of methionine, pyroglutamine on peptide amino termini, and protein N-terminal acetylation were set as variable modifications. A precursor mass tolerance of 5 ppm and a fragment ion quantification tolerance of 20 ppm were used. Data were compared in a semi-quantitative manner using the number of spectral counts per protein. Individual protein values were normalized to the total number of spectral counts identified in that sample.

Proximity Ligation Assay

In situ protein interactions were detected by the DuoLink In Situ Red (or Green) Starter Kit Mouse/Rabbit (# DUO92101; #DUO92014; Sigma-Aldrich) according to the manufacturer's protocol. Cells were grown on Nunc Lab-Tek II CC^2 eight-well chamber slides (#154534PK; Thermo Fisher Scientific) for 24 hours, fixed with 4% paraformaldehyde, and permeabilized with 0.5% Triton X-100. For the mitochondrial staining, cells were incubated with 150 nM MitoTracker CMX Ros (#M7512; Thermo Fisher Scientific) for 10 minutes at room temperature before fixation. Cells were blocked with Duolink Blocking Solution for 1 hour at 37°C and then incubated overnight at 4°C with primary antibodies for anti-HA (mouse, #901501; BioLegend) and anti-HSP90 (rabbit, #ab13495; Abcam), anti-HSC70 (rabbit, #PA5-27337; Invitrogen), or anti-TOM70 (rabbit, #14528-1-AP; Thermo Fisher Scientific). Secondary antibodies conjugated with Duolink PLA Plus (donkey anti-mouse) and Minus (donkey anti-rabbit) oligonucleotides probes were incubated for 1 hour at 37°C. Cell membranes were stained with 1 µg/mL of CF640-conjugated wheat germ agglutinin (#29026; Biotium, Fremont, CA, USA) in 0.01× Washing Buffer B for 10 minutes at room temperature. Cells were mounted with a drop of Duolink Mounting Media with DAPI (#DUO82040; Sigma-Aldrich). The proximity ligation assay (PLA) signals were analyzed by Zeiss LSM 800 confocal microscopy (Zeiss, Oberkochen, Germany) with Airyscan (63× objective, 1.8× zoom). The number of PLA puncta per cell were quantified from a single image plane using the "Analyze Particles" feature of ImageJ software (National Institutes of Health, Bethesda, MS, USA) with at least 45 cells counted from 8 to 11 fields of view for each sample.

Immunoblot Analysis

Whole cells/isolated mitochondria from cells were lysed in ice-cold 1× RIPA buffer (#9806; Cell Signaling Technology) with addition of 1 mM PMSF (#8553; Cell Signaling Technology) immediately before use. Then, 15 µg of lysates for whole cells, mitochondrial or cytosolic fraction (supernatant) was resolved by SDS-PAGEs and then transferred to a polyvinylidene difluoride membrane. Membranes were blocked with 5% nonfat dried milk in TBST and incubated overnight at 4°C with the indicated primary antibodies. Secondary antibodies were applied for 1 hour at room temperature. Primary antibodies used were HA tag (#901501; BioLegend), SLC4A11 (custom[33]; detects all isoforms SLC4A11-A, SLC4A11-B, and SLC4A11-C; see Supplementary Fig. S4b), HSP90 (#sc-13119; SCBT, Dallas, TX, USA), HSC70 (#sc-7298; SCBT), VDAC (#ab15895; Abcam, Cambridge, MA, USA), ANT (#ab102032; Abcam), RISP (#sc-271609; SCBT), COXIV (#4850; CST, Danvers, MA, USA), TOM70 (#sc-390545; SCBT), α-tubulin (#sc-8035; SCBT), GAPDH (#sc-32233; SCBT), and β-actin (#A5441; Sigma-Aldrich). The immunoreactive bands were visualized by enhanced chemiluminescence, ECL buffer (#34578; Thermo Fisher Scientific), using the Gel Doc XR+ system (Bio-Rad, Hercules, CA, USA).

Immunoprecipitation

Immunoprecipitation was conducted according to the manufacturer's protocol (#26146; Thermo Fisher Scientific). Whole cells/isolated mitochondria from PS120-hSLC4A11-HA and -EV cells were lysed in ice-cold immunoprecipitation (IP) lysis/wash buffer (0.025 M Tris, 0.15M NaCl, 0.001M EDTA, 1% NP-40, 5% glycerol, pH 7.4) supplemented with 1× protease/phosphatase inhibitor cocktail (#5872; Cell Signaling Technology). Then, 5 µg of an antibody specific to an antigen of interest or a nonimmune mouse IgG control was incubated with 1 mg of the precleared whole-cell/mitochondrial lysates overnight at 4°C. The following antibodies were used for IP: HA tag (#901501; BioLegend), HSP90 (#sc-13119; SCBT), HSC70 (#sc-7298; SCBT), TOM70 (#sc-390545; SCBT), and mouse IgG control (#10400C; Thermo Fisher Scientific). The immune complex from the resins was eluted by incubation with 2× sample buffer (0.5 M Tris-HCl [pH 6.8], 4.4% [w/v] SDS, 20% [v/v] glycerol, 2% [v/v] 2-mercaptoethanol, and bromophenol blue in distilled

Investigative Ophthalmology & Visual Science

water) at 100°C for 10 minutes, and the precipitates were resolved on SDS-PAGE gels.

In Vitro HSP90 Inhibitor Study on Mitochondrial SLC4A11 Transport

Cells were seeded in T175 flasks, cultured in Complete Media at 37°C for 24 hours, and treated with 18 µM geldanamycin (#sc-200617; Santa Cruz, Dallas, TX, USA) for an indicated time. For novobiocin treatment (#sc-358734; Santa Cruz), cells were treated with the inhibitor at different concentrations (10, 100, 300, and 500 µM) for 6 hours. Dimethyl sulfoxide (DMSO) and H_2O were used as a control for geldanamycin and novobiocin treatments, respectively. After treatment, cells were washed twice with PBS, scraped with a cell lifter, and pelleted by centrifugation at 500 × *g* for 5 minutes, followed by purification of mitochondria and immunoblotting of mitochondrial and supernatant fraction, as described above.

Small Interfering RNA Transfection

Small interfering RNAs (siRNAs) of HSC70 (#NM_006597) and MISSION siRNA Universal Negative Control #1 (#SIC001-10NMOL) were purchased from Sigma-Aldrich. siRNAs targeting human HSP90 (#sc-35608) and mouse HSP90 (#sc-35610) were obtained from Santa Cruz. Cells were transfected using Lipofectamine RNAiMAX Transfection reagent (#13778075; Invitrogen, Carlsbad, CA, USA) according to the manufacturer's protocol. After 68 hours of transfection at 37°C, cells were harvested for mitochondrial purification for the immunoblotting analysis or cell/isolated mitochondria Mito Stress Test on a Seahorse XFe24 Analyzer (Agilent, Santa Clara, CA, USA).

Mitochondrial Purification From *Slc4a11* WT and KO Mice Kidneys

Fresh kidneys from *Slc4a11* WT and KO mice were harvested at termination and rinsed with PBS, and renal capsules were immediately removed. The kidneys were thoroughly minced in ice-cold mitochondrial isolation buffer (MIB-1; 10 mM Tris-MOPS, 1 mM EGTA-Tris, 200 mM sucrose, pH 7.4, supplemented with complete protease inhibitor cocktail [#11697498001; Roche]) to wash away blood and rinsed three more times with fresh MIB-1. All steps were performed at 4°C. The kidney pieces in the ratio 10 mL of MIB-1 buffer per gram of kidney (i.e., 10:1, v:w) were ruptured with a prechilled Dounce glass homogenizer, followed by centrifugation at 800 × *g* for 10 minutes at 4°C. The pellet containing unbroken cells and nuclei was discarded, and the supernatant was centrifuged at 10,000 × *g* for 15 minutes at 4°C to pellet the mitochondria-enriched fraction. This pellet was washed in ice-cold IB-2 and centrifuged at 10,000 × *g* for 15 minutes at 4°C. The final pellet containing mitochondria was gently resuspended in IB-2. The supernatant containing mostly cytoplasmic and plasma membrane proteins was saved as a cytosolic fraction indicator.

Ex Vivo Kidney HSP90 Inhibitor Study on Mitochondrial Slc4a11 Transport

To enhance drug penetration, approximately 15 holes were made in *Slc4a11* WT kidneys using a 31-gauge needle and then preconditioned with 20 mg/kg novobiocin in Hank's balanced salt solution (HBSS) containing 0.5% BSA for 15, 30, or 60 minutes at 37°C. Control kidneys were incubated in HBSS containing 0.5% BSA. The kidneys were washed two times in HBSS, followed by mitochondrial purification assay and immunoblotting of the mitochondrial and supernatant fraction.

Mitochondrial Function Measurements Using Seahorse XFe24

The mitochondrial bioenergetics of live cells and isolated mitochondria were determined through the real-time measurement of oxygen consumption rate (OCR) using a Seahorse XFe24 Analyzer (Agilent). For a cell mitochondrial stress test, MCECs were seeded onto FNC (#0407; Athena Enzyme Systems, Baltimore, MD)-coated XF24 microplates (#100777-004; Agilent) in an antibiotic-free complete medium overnight and transfected with the indicated siRNAs for 48 hours, followed by incubation in an assay media containing DMEM (no glucose, no glutamine, no sodium pyruvate, no phenol red) (#A14430-01; Thermo Fisher Scientific), 1 g/L glucose (#A24940-01; Thermo Fisher Scientific) ± 0.5 mM glutamine (#250030-081; Thermo Fisher Scientific), and 0.5% dialyzed FBS (#26400-036; Thermo Fisher Scientific) for 20 hours at 33°C. On the day of analysis, the medium was replaced with XF Base Medium (#102353-100; Agilent), supplemented with 1g/L glucose and 0.5 mM glutamine, and cells were incubated for 45 minutes in a non-CO_2 37°C incubator. Each compound from a Mito Stress Test Kit (#103010-100; Agilent) was sequentially injected in the well set to a final concentration: 2 µM oligomycin, 0.5 µM carbonyl cyanide-*p*-trifluoromethoxyphenylhydrazone (FCCP), and 0.5 µM rotenone and antimycin A. Three OCR measurements were conducted each for baseline, followed by injection of oligomycin, FCCP, and rotenone and antimycin A, respectively. After assay, cell number per each well was counted after trypsinizing the cells plated on the XF24 microplates and used to normalize the OCR.

For the purified mitochondrial bioenergetics, MCECs were transfected with the indicated siRNAs for 48 hours, followed by incubation in an assay media for 20 hours at 33°C. Then, 10 µg of isolated mitochondria in 50 µL of cold Mitochondrial Assay Solution (MAS; 70 mM sucrose, 190 mM mannitol, 10 mM KH_2PO_4, 5 mM $MgCl_2$, 2 mM HEPS, 1 mM EGTA, 5 mM NaCl, 20 mM taurine, 100 µM NAD, 100 µM $NADP^+$, and 0.2% [w/v] fatty acid-free BSA, pH 7.2) supplemented with respiratory substrates (10mM pyruvic acid and 2mM malic acid) was loaded into XF24 microplates (#100777-004; Agilent) and spun at 2000 × *g* for 20 minutes at 4°C. After centrifugation, 450 µL of prewarmed MAS containing respiratory substrates (10 mM pyruvic acid and 2 mM malic acid) ± 4 mM glutamine (#103579-100; Agilent) was added to each well. OCR was measured three times each for baseline, followed by consecutive addition of 2 mM adenosine diphosphate (ADP), 3 µM oligomycin, 4 µM FCCP, and 4 µM rotenone and antimycin A (set to final concentration per well).

For the purified mitochondrial bioenergetics from *Slc4a11* WT and KO kidneys, 10 µg mitochondria in 50 µL cold MAS containing respiratory substrates (10 mM pyruvic acid and 2 mM malic acid) was loaded into XF24 microplates (#100777-004; Agilent) and spun at 2000 × *g* for 20 minutes at 4°C, followed by addition of 450 µL prewarmed

Investigative Ophthalmology & Visual Science

MAS containing respiratory substrates (10 mM pyruvic acid and 2 mM malic acid) ± 4 mM glutamine (#103579-100; Agilent) to each well. OCR was measured three times each for baseline following sequential injections of 3 mM ADP, 3 µM oligomycin, 4 µM FCCP, and 4 µM rotenone and antimycin A, respectively (final concentration per well).

After assay with isolated mitochondria, mitochondria from all wells were viewed under the phase contrast using an EVOS FL Auto Imaging System (Thermo Fisher Scientific) to ensure consistent adherence to the well even after the assay (see Supplementary Fig. S4c). All data were analyzed using XFe Wave (Agilent) and GraphPad Prime 8.0 (GraphPad Software, La Jolla, CA, USA).

Ammonia Production Assay

A total of 1×10^5 MCEC cells/well were plated into 12-well plates in antibiotic-free complete medium overnight, transfected with 50 nM of the indicated siRNAs for 48 hours, and then incubated with an assay media for 20 hours at 33°C. After 68 hours posttransfection, medium supernatant was collected and centrifuged at 500 × *g* for 5 minutes to remove debris. The supernatant was measured for ammonia concentration with an Ammonia Colorimetric Assay Kit (#K370-100; Biovision, Milpitas, CA, USA).

Flow Cytometric Analysis for Mitochondrial ROS Level

MCECs were prepared using the same protocol as described for the ammonia production assay and harvested after 68 hours posttransfection. Mitochondrial superoxide was detected using the MitoSOX Red probe (#M36008; Thermo Fisher Scientific). Cells were incubated in HBSS with 2.5 µM MitoSOX Red for 25 minutes at 37°C, washed with prewarmed HBSS, and resuspended in HBSS. Cells were filtered through 50-µm sterile CellTrics Filters (#04-004-2327; Sysmex, Lincolnshire, IL, USA) for flow cytometry analysis. Cells were analyzed using a four-laser LSRII flow cytometer (BD Biosciences, San Jose, CA) equipped with a 488-nm 30-mW laser for forward scatter (FSC) and side scatter (SSC) detection and a 561-nm laser, 582/15 emission filter for MitoSOX detection. Cells were gated based on light scatter (FSC-A versus SSC-A) and single-cell (FSC-A versus FSC-H) characteristics, and 10,000 single cells per sample were saved for fluorescence analysis. Data were collected using FACSDiva 6.1.3 software (BD Biosciences) and analyzed using FlowJo software 10.7.1 (FlowJo LLC, Ashland, OR, USA).

Statistical Analysis

All analyses were performed in triplicate or more unless otherwise stated. Statistical analysis and graphical illustrations were performed using GraphPad Prime 8.0 (GraphPad Software). The data given in figures and text are expressed as mean ± SEM. A two-tailed Welch's test was applied for two-group comparison. A one-way ANOVA or two-way ANOVA followed by multiple comparisons test (Tukey, Bonferroni, or Dunnett) was used for data of more than two groups. A *P* value of <0.0032 (* or δ), <0.0021 (** or $\delta\delta$), <0.0002 (*** or $\delta\delta\delta$), and <0.0001 (**** or $\delta\delta\delta\delta$) was considered statistically significant and asterisked in the relevant plots.

Results

Mitochondrial SLC4A11 Import Is Not via the Presequence Pathway

As an initial step toward elucidating the underlying mechanisms of SLC4A11 trafficking to the mitochondria, in silico mitochondrial proteomic analyses from MitoProt II,[28,29] TargetP2.0,[30] Predotar,[32] and iPSORT[31] predict potential trafficking pathways by examining the existence of the N-terminal canonical mitochondrial targeting sequence. Five well-annotated mitochondrial proteins having canonical targeting sequences at the N-terminus (SIRT3,[34] SOD2,[35] HSP60,[36] GLS2,[37] and RISP[38]) were used as positive controls (Fig. 1a). Herein, along with all three isoforms of SLC4A11,[12] three newly discovered proteins that have cytoplasmic and mitochondrial distribution (SOD1,[39] Akt,[40] and SIRT1[41]) had low probabilities of import to the mitochondria based on the N-terminal targeting sequence. Figure 1a shows that SLC4A11 is also similar to other well-known mitochondrial membrane proteins having cryptic internal signals, ANT1[20,42] and UCP2[43] (see also Supplementary Fig. S1a).[28–32] Since SLC4A11 is in mitochondria, this finding raised the possibility that mitochondrial SLC4A11 could have cryptic internal signals and traffic to the IMM through the carrier pathway, which uses specific molecular chaperones in cytosolic and mitochondrial intermembrane spaces.[19,21]

We next screened for potential interactors of SLC4A11 on the mitochondria surface. PS120 hamster fibroblasts stably transfected with either N-terminal HA-tagged human-SLC4A11 isoform B (hSLC4A11-HA) or EV were treated with the thiol crosslinking agent DSP and lysate peptides analyzed by LC-MS/MS, as illustrated in Figure 1b. Using either whole-cell or isolated mitochondria lysates, SLC4A11-HA–interacting proteins were immunoprecipitated using HA antibody (Fig. 1c) and identified by untargeted LC-MS/MS analysis. Figure 1d shows that HSC70 and HSP90 were the only proteins observed to be at least twofold higher in isolated mitochondria from SLC4A11-transfected cells than in mitochondria from EV-transfected cells (Supplementary Fig. S1b). HSP90β was shown to be associated with SLC4A11 protein from PS120-hSLC4A11-HA whole cells relative to PS120-EV (Supplementary Fig. S1c). Thus, we selected HSP90 and HSC70 as putative candidates that would bind to SLC4A11 and further demonstrated their role in targeting mitochondrial SLC4A11 import.

To determine whether the leading candidates observed from LC-MS/MS correspond to physical interaction with SLC4A11, SLC4A11 and either HSP90 or HSC70 were analyzed by PLA, which visualizes the in situ protein–protein localization.[44] Anti-HA antibody was paired with either anti-HSP90 or anti-HSC70 antibodies in PS120-hSLC4A11-HA or -EV. Hybridized and amplified primary antibody-linked oligonucleotides (PLA probes) can be detected by fluorescence signal only when the antibodies are in very close proximity to each other (<40 nm).[44,45] We found robust HA/HSP90 as well as HA/HSC70 PLA signals in PS120-hSLC4A11-HA cells relative to PS120-EV cells and a no 1° antibody negative control (Figs. 1e–g and Supplementary Fig. S2b). These data reveal that SLC4A11 can bind to the molecular chaperones HSP90 and HSC70, suggesting the possibility that mitochondrial SLC4A11 import follows a carrier pathway.

Investigative Ophthalmology & Visual Science

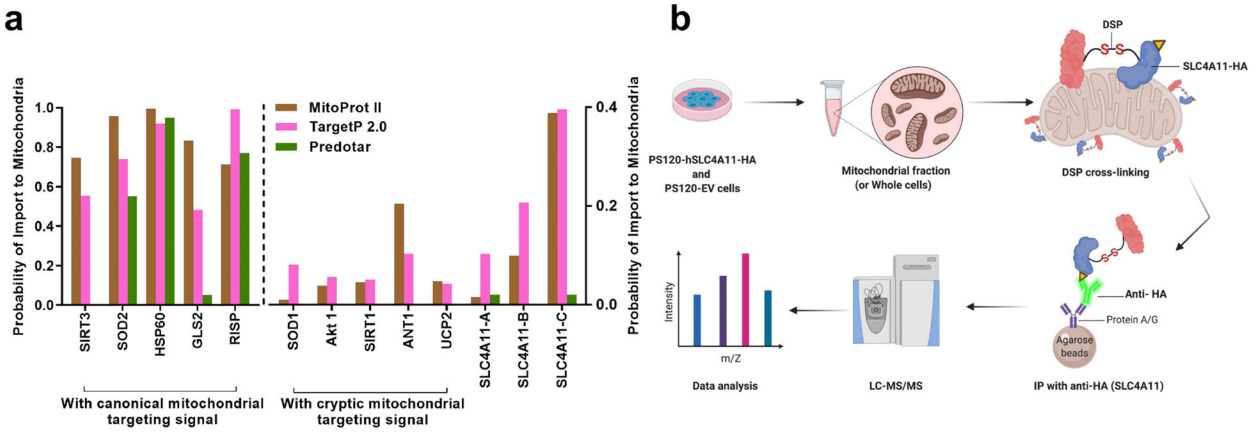

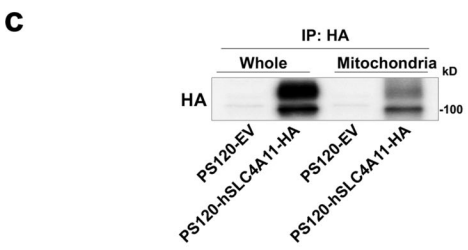

d

Mitochondria

Protein	Peptide count	
	EV	SLC4A11-HA
SLC4A11	0	6.51
HSC70	2.17	5.72
HSP90 α	0.46	1.32
HSP90 β	0.42	0.97

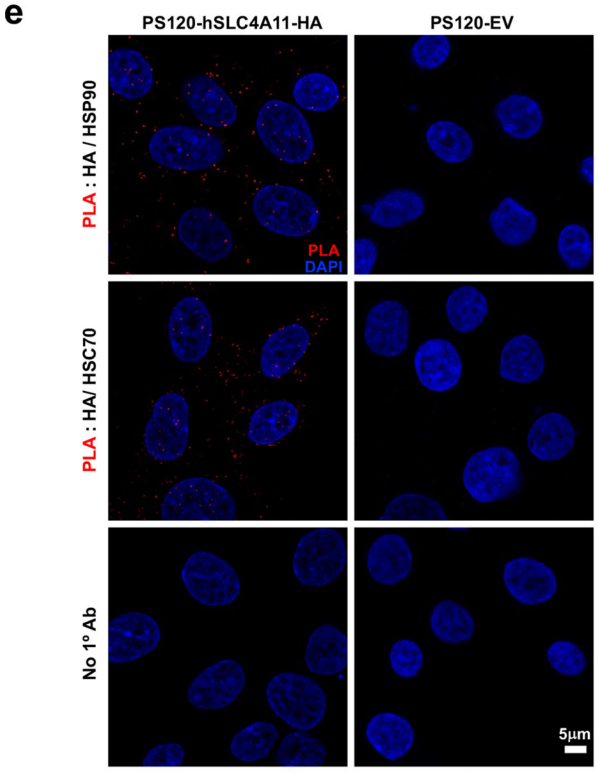

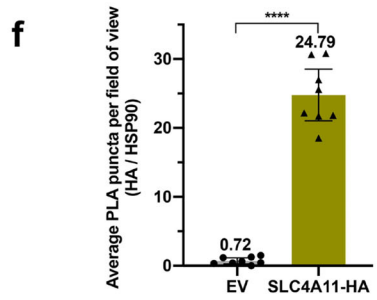

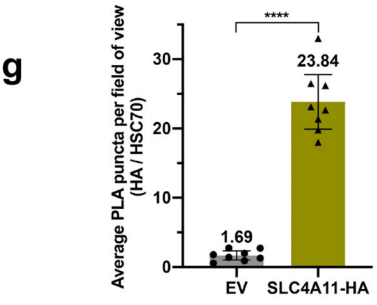

Figure 1. Chaperone-mediated carrier pathway for mitochondrial SLC4A11 import. (**a**) In silico proteomic screening for the presence of an N-terminal mitochondrial targeting signal of all three isoforms of SLC4A11 (-A, -B, and -C) together with other mitochondrial proteins. The graph shows the probability, ranging from 0 to 1, of having N-terminal mitochondrial targeting signals. (**b**) Experimental procedure flowchart: SLC4A11-interacting proteins were crosslinked with SLC4A11 using a DSP crosslinker in whole-cell or isolated mitochondrial lysates from PS120 fibroblasts transfected with EV or human SLC4A11 tagged with HA epitope (hSLC4A11-HA) and immunoprecipitated with anti-HA antibody. Peptide sequences of SLC4A11-binding proteins were analyzed by untargeted LC-MS/MS analysis. (**c**) Validation of efficient SLC4A11-HA immunoprecipitation coupled with DSP crosslinking in whole-cell and isolated mitochondrial lysates was analyzed by immunoblotting before LC-MS/MS analysis. (**d**) Putative protein candidates bound to SLC4A11 on mitochondria of PS120-hSLC4A11-HA cells, identified by LC-MS/MS analysis as HSP90 and HSC70: average peptide counts of individual protein from three replicates are shown in the table. Raw data are shown in Supplementary Figure S1b. (**e**) Representative confocal images of HA/HSP90- and HA/HSC70-PLA (*red*) and DAPI (*blue*) from $n = 8$ fields of view in PS120-hSLC4A11-HA and PS120-EV cells. *Scale bar*: 5 µm. (**f**, **g**) Quantification of HA/HSP90 and HA/HSC70-PLA signal from (**e**). Each symbol represents average number of PLA puncta per each field of view ($n = 8$). Mean values ± SEM are present above *bar* and significances were tested against the corresponding PS120-EV cells by a two-tailed Welch's *t*-test. ****$P < 0.0001$.

Investigative Ophthalmology & Visual Science

HSP90 and HSC70 Chaperones Participate in Assisting SLC4A11 Transfer to the Outer Mitochondrial Membrane

To further investigate whether HSC70 and HSP90 participate in SLC4A11 protein targeting to mitochondria, we tested the interaction between these chaperone proteins with HA-tagged SLC4A11 by anti-HA IP. We found that coimmunoprecipitation with HA-SLC4A11, HSP90, and HSC70 antibodies in both whole cells (Fig. 2a) and isolated mitochondria (Fig. 2b) from PS120-hSLC4A11-HA cells revealed that SLC4A11 and HSP90/HSC70 direct interactions are present in both the cytoplasm and mitochondria. Previous studies have demonstrated that docking HSP90 and/or HSP70 onto TOM70 is essential for the targeting of mitochondrial precursors having multiple internal signals to the import pore of TOM complexes.[20,21] Figure 2b shows that HSP90 as well as HSC70 could pull down TOM70. Also, a direct physical interaction between SLC4A11 and TOM70 was found by reciprocal coimmunoprecipitation from PS120-hSLC4A11-HA mitochondrial lysates. Consistent with these findings, PLA revealed significant colocalization of SLC4A11 with TOM70 in PS120-hSLC4A11-HA cells but not in PS120-EV cells (Figs. 2c, 2d). Overall, these results support HSP90, HSC70, and TOM70 as physical binding partners with SLC4A11, suggesting a possible role of the chaperones (HSP90/HSC70) in SLC4A11-HSP90/HSC70 complexes recruited in the cytoplasm to deliver SLC4A11 to the mitochondrial surface through TOM70.

SLC4A11–Chaperone (HSP90 and/or HSC70) Complexes Are Targeted to Outer Mitochondrial Membrane, Specifically to TOM70

Evidence suggesting that HSP90, HSC70, and TOM70 bind to SLC4A11 prompted us to further explore the localization of SLC4A11–chaperone complexes with mitochondria. Cells were labeled with MitoTracker CMXRos prior to PLA. Figures 3a and 3b (open arrows) show that more than half of the HA/HSP90 PLA signal was visualized as single green dots in the cytoplasm as expected, where initial interactions would occur. The rest of the discrete HA/HSP90 PLA puncta colocalized with mitochondria or were in close contact with the surface of mitochondria, showing an overlapping yellow signal (Fig. 3b, arrows). We observed a similar distribution pattern of HA/HSC70 PLA signals at the mitochondria and cytosol (Figs. 3c, 3d). Since TOM70 is the outer mitochondrial membrane protein, TOM70 staining does circumscribe inner matrix MitoTracker CMXRos staining (Supplementary Fig. S2a). Notably, most PLA puncta for HA/TOM70 interactions showed overlapping localization to the mitochondria (Figs. 3e, 3f). Consistent with direct interaction between SLC4A11 and TOM70 in a reciprocal pull-down assay (Fig. 2b), it indicates that TOM70 is most closely a direct binding receptor for mitochondrial SLC4A11 translocation. No PLA signal was detected in negative control samples incubating with a single primary antibody or no primary antibody (Supplementary Figs. S2b, S2c). Overall, immunofluorescence colocalization of HA/HSP90, HA/HSC70, and HA/TOM70 PLA puncta with mitochondrial staining validated that HSP90 and/or HSC70 are the cytosolic chaperones, which allow SLC4A11 to traverse across the mitochondria through specific binding to TOM70.

Inactivation of the Chaperone Function Inhibits Mitochondrial SLC4A11 Translocation

After establishing that HSP90 and HSC70 are associated with SLC4A11 mitochondrial targeting, we inhibited the function of HSP90 and knocked down the expression of HSP90 or HSC70 to demonstrate functional interaction. We first applied geldanamycin, an HSP90 ATPase inhibitor for both HSP90α and HSP90β, which is widely used in studies of mitochondrial precursor import.[20,21,46,47] In the presence of 18 µM geldanamycin, mitochondria from PS120-hSLC4A11-HA cells (Fig. 4a) and WT MCECs (Supplementary Fig. S3a) showed gradually diminishing levels of SLC4A11 (HA tagged or endogenous, respectively) in the mitochondria over time, suggesting there is an impairment of the import of SLC4A11 into the mitochondria. For verification of HSP90 inhibitor specificity on mitochondrial SLC4A11 translocation, another selective HSP90 inhibitor, novobiocin,[20,48] was tested in both *Slc4a11* WT MCECs (Fig. 4c) and PS120-hSLC4A11-HA cells (Supplementary Fig. S3b), and purified mitochondria were analyzed by Western blotting. The mechanism of novobiocin action has been shown to reduce precursor interactions with HSP90, resulting in blockage of TOM70 targeting.[20] Similar to geldanamycin, novobiocin decreased SLC4A11 translocation to the mitochondria. As expected, the distribution pattern of mitochondrial SLC4A11 after either geldanamycin or novobiocin treatment was very closely linked to the TOM70-dependent mitochondrial protein, adenine nucleotide translocator (ANT),[20,42] but not to the TOM70-independent Rieske iron–sulfur protein (RISP)[38] (Figs. 4b, 4d). In agreement with HSP90 inhibitor studies, reducing HSP90 expression in HCECs (Fig. 4e and Supplementary Fig. S3c) and WT MCECs by siRNA (Supplementary Fig. S3e) resulted in significant suppression of SLC4A11 translocation to mitochondria. Consistent with data shown in Figure 4e and Supplementary Figure S3e, a similar effect was observed in mitochondrial fractions isolated from HCECs that were transfected with HSC70 siRNA (Fig. 4f and Supplementary Fig. S3d). Thus, these results demonstrate that HSP90 and HSC70 are required for recruiting SLC4A11–chaperone complexes, which in turn target SLC4A11 to the mitochondria.

Slc4a11 Is Present in Kidney Mitochondria and Facilitates Gln Catabolism

Slc4a11 KO mice also exhibit renal abnormalities, including polyuria with low urine osmolality.[10,11] SLC4A11 is highly expressed in the proximal tubule,[7,10] where numerous mitochondria are present and adenosine triphosphate (ATP) production relies on mitochondrial oxidative phosphorylation fueled mainly by Gln and free fatty acids.[49] We first examined the weight and size of kidneys as this is often a potential surrogate measure of dysfunction. We observed that the kidney to body weight ratio was reduced in *Slc4a11* KO mice at 8-week-old relative to *Slc4a11* WT mice, in both male and female mice (Figs. 5a, 5b). However, we did not find histomorphologic differences within the renal tissue structure by hematoxylin and eosin staining (data not shown). To determine if Slc4a11 expression facilitates Gln catabolism in the kidney, we examined oxygen consumption of kidney mitochondria isolated from WT and KO mice. Figure 5c shows that basal oxygen consumption of WT and KO mitochondria was similar in the absence of Gln. However, in the presence of Gln, oxygen consumption

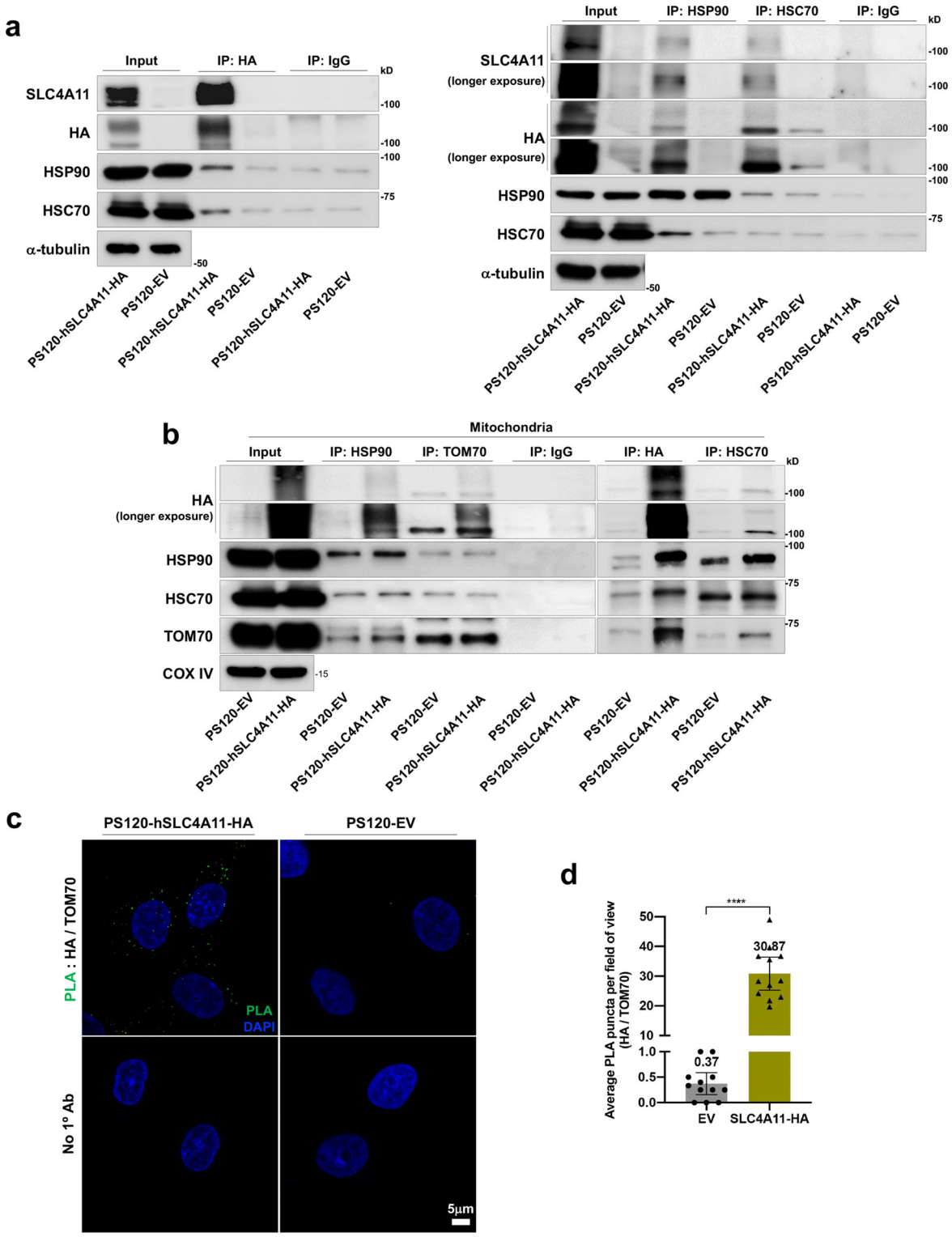

Figure 2. HSP90 and HSC70 chaperones are SLC4A11-binding partners assisting transfer to the outer mitochondrial membrane. (**a**) Reciprocal coimmunoprecipitation to determine cytosolic chaperones that bind to SLC4A11. Whole-cell lysates from PS120-EV and PS120-hSLC4A11-HA cells were immunoprecipitated with an antibody specific for the corresponding proteins, as indicated. The immunocomplexes were analyzed by Western blotting using indicated antibodies. A mouse IgG control was used as a negative control. Input comprised preimmunoprecipitated whole-cells lysates that were blotted to check the molecular weight of each protein as a positive control. Representative Western blots of three independent experiments. (**b**) Western blotting of reciprocal coimmunoprecipitations conducted with mitochondrial lysates from PS120-EV and PS120-hSLC4A11-HA cells showing that HSP90 and HSC70 are the SLC4A11-binding proteins on the mitochondria in PS120-hSLC4A11-HA cells, and all three proteins are directly bound to TOM70. Representative Western blots of three independent experiments. (**c**) Representative confocal images of HA/TOM70-PLA (*green*) puncta in PS120-hSLC4A11-HA and PS120-EV cells. A nuclear counterstain marker was labeled in *blue* with DAPI. $n = 12$ fields of view per condition. *Scale bars*: 5 µm. (**d**) Quantification of HA/TOM70-PLA signals from panel (**e**). Each symbol represents average number of PLA puncta per each field of view ($n = 12$). Mean values ± SEM are present above the *bar* and significances were tested against the corresponding PS120-EV cells by a two-tailed Welch's *t*-test. ****$P < 0.0001$.

Investigative Ophthalmology & Visual Science

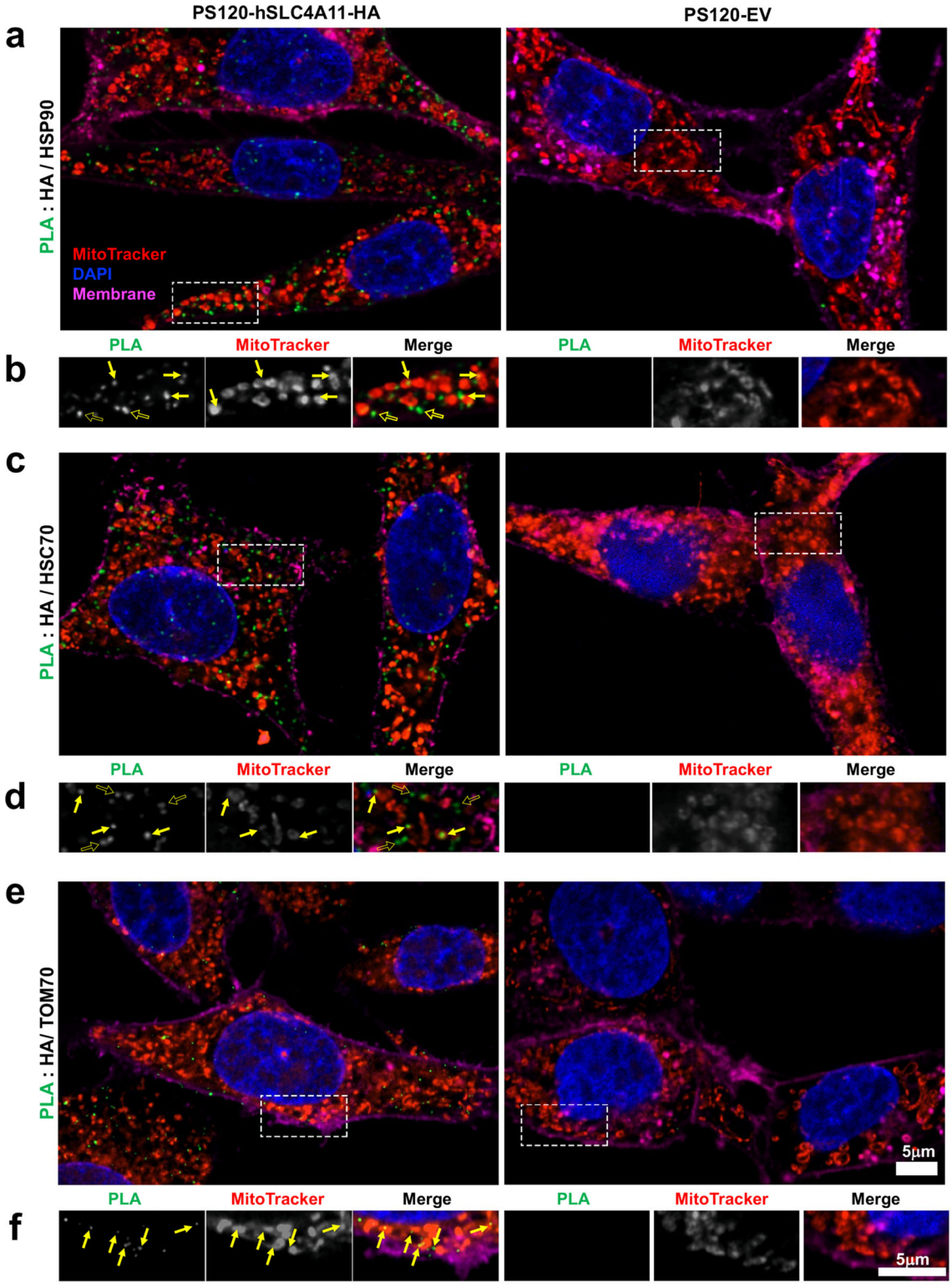

Figure 3. SLC4A11–chaperone (HSP90 or HSC70) complexes are targeted to outer mitochondrial membrane (OMM), specifically to TOM70. (**a**) Representative confocal images showing the colocalization of HA/HSP90-PLA (*green*) signals with mitochondria, labeled with MitoTracker CMXRos (*red*) in PS120-hSLC4A11-HA and PS120-EV cells. (**b**) Inserts from panel (**a**) showing magnified merged images. *Open arrows*: *green* PLA puncta in the cell cytoplasm. *Arrows*: colocalization of HSP90 and SLC4A11-HA puncta along the mitochondria. (**c**) Representative confocal images showing the colocalization of HA/HSC70-PLA (*green*) signals with mitochondria, labeled with MitoTracker CMXRos (*red*) in PS120-hSLC4A11-HA and PS120-EV cells. (**d**) Inserts from panel (**c**) showing magnified merged images. *Open arrows*: *green* PLA puncta in the cell cytoplasm. *Arrows*: colocalization of HSC70 and SLC4A11-HA puncta along the mitochondria. (**e**) Representative confocal images showing the colocalization of HA/TOM70-PLA (*green*) signals with mitochondria, labeled with MitoTracker CMXRos (*red*) in PS120-hSLC4A11-HA and PS120-EV cells. (**f**) Inserts from panel (**e**) showing magnified merged images. *Arrows*: colocalization of TOM70 and SLC4A11-HA puncta along the mitochondria. All cells were stained with CF640-conjugated wheat germ agglutinin (WGA) (*pink*) to label the cell membranes and with DAPI (*blue*) as a nuclear counterstain marker. $n = 10$ fields of view per condition. *Scale bars*: 5 µm.

Investigative Ophthalmology & Visual Science

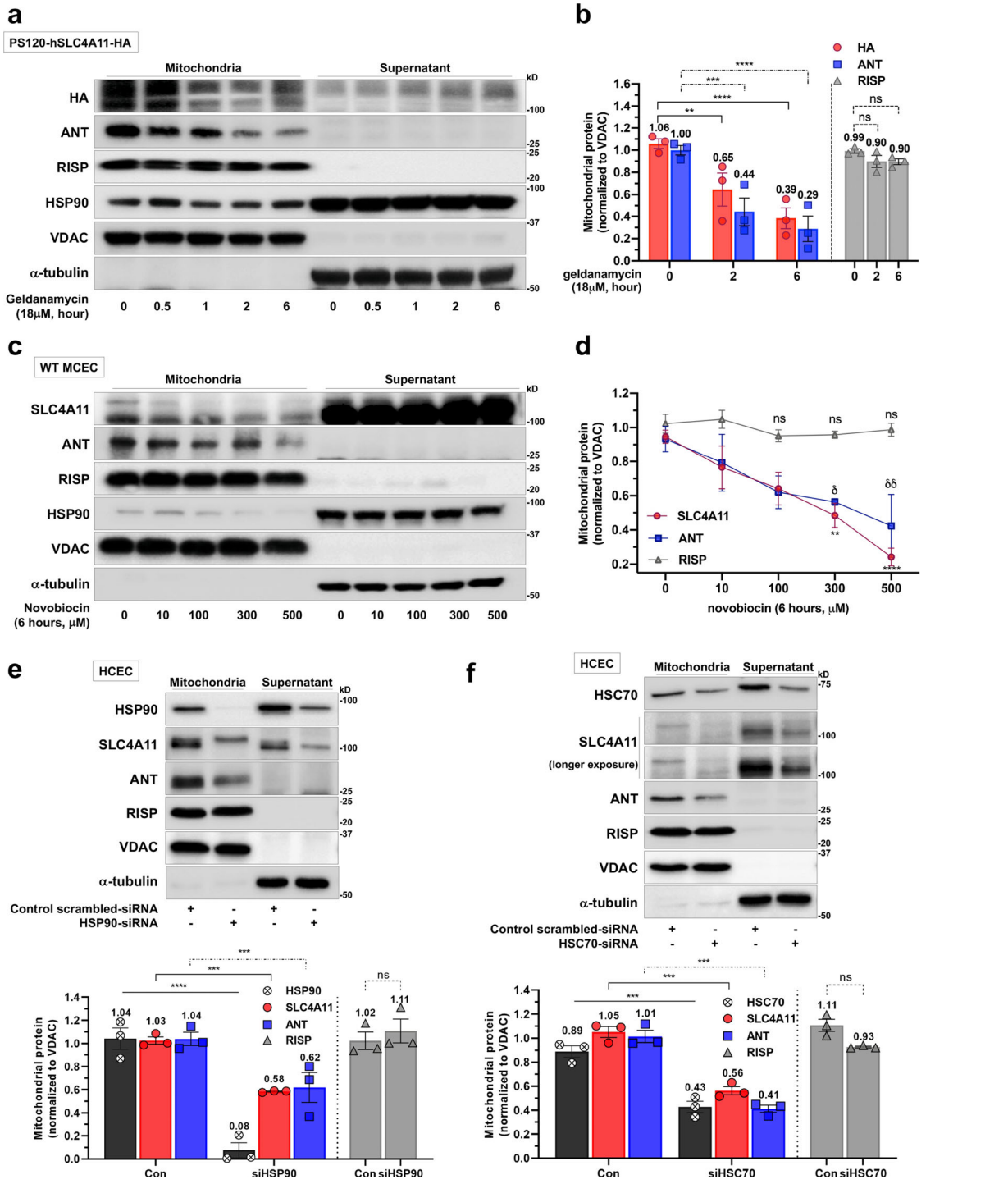

Figure 4. Inactivation of the chaperone function interrupts mitochondrial SLC4A11 translocation. (**a**) The extent of mitochondrial SLC4A11 transport in the presence of HSP90 inhibitors geldanamycin was analyzed by immunoblotting of mitochondrial and supernatant (cytoplasmic) fractions from PS120-hSLC4A11-HA. The TOM70-dependent mitochondrial protein, ANT, and the TOM70-independent protein, RISP, were probed as positive and negative controls, respectively. The levels of VDAC served as a mitochondrial marker. α-Tubulin is a loading control for cytoplasmic fraction. (**b**) Immunoblots of mitochondrial fraction from (**a**) were normalized relative to VDAC. Quantification is reported in relative to initial time point. (**c**) Immunoblotting of each fraction from WT MCECs that were treated with increasing concentrations of HSP90 inhibitor novobiocin for 6 hours. (**d**) Quantification of Western blots of mitochondrial fraction from (**c**). Mean values ± SEM. $n = 3$ (*P value versus 0 μM, SLC4A11; δ P value versus 0 μM, ANT). (**e**) Immunoblotting analysis of each fraction from HCECs that were transfected with control scrambled siRNA or HSP90 siRNA for 68 hours. Mitochondrial SLC4A11 transport was interrupted by HSP90 knockdown. Efficiency of HSP90 knockdown in HCECs analyzed by immunoblotting is shown in Supplementary Figure S3c. *Bottom*: quantification of Western blots of mitochondrial fraction. (**f**) Immunoblotting analysis of each fraction from HCECs that were transfected with either control scrambled siRNA or HSC70 siRNA for 68 hours, showing interruption of mitochondrial SLC4A11 transport by HSC70 knockdown. For validation of efficient HSC70 siRNA delivery, see Supplementary Figure S3d. *Bottom*: quantification of Western blots of mitochondrial fraction. Data are presented as mean ± SEM from $n = 3$ independent experiments. *$P < 0.0332$, **$P < 0.0021$, ***$P < 0.0002$, ****$P < 0.0001$ and ns = not significant, two-way ANOVA with Dunnett's multiple comparison (for **b**, **d**) and two-way ANOVA with a Bonferroni's multiple comparison (for **e**, **f**).

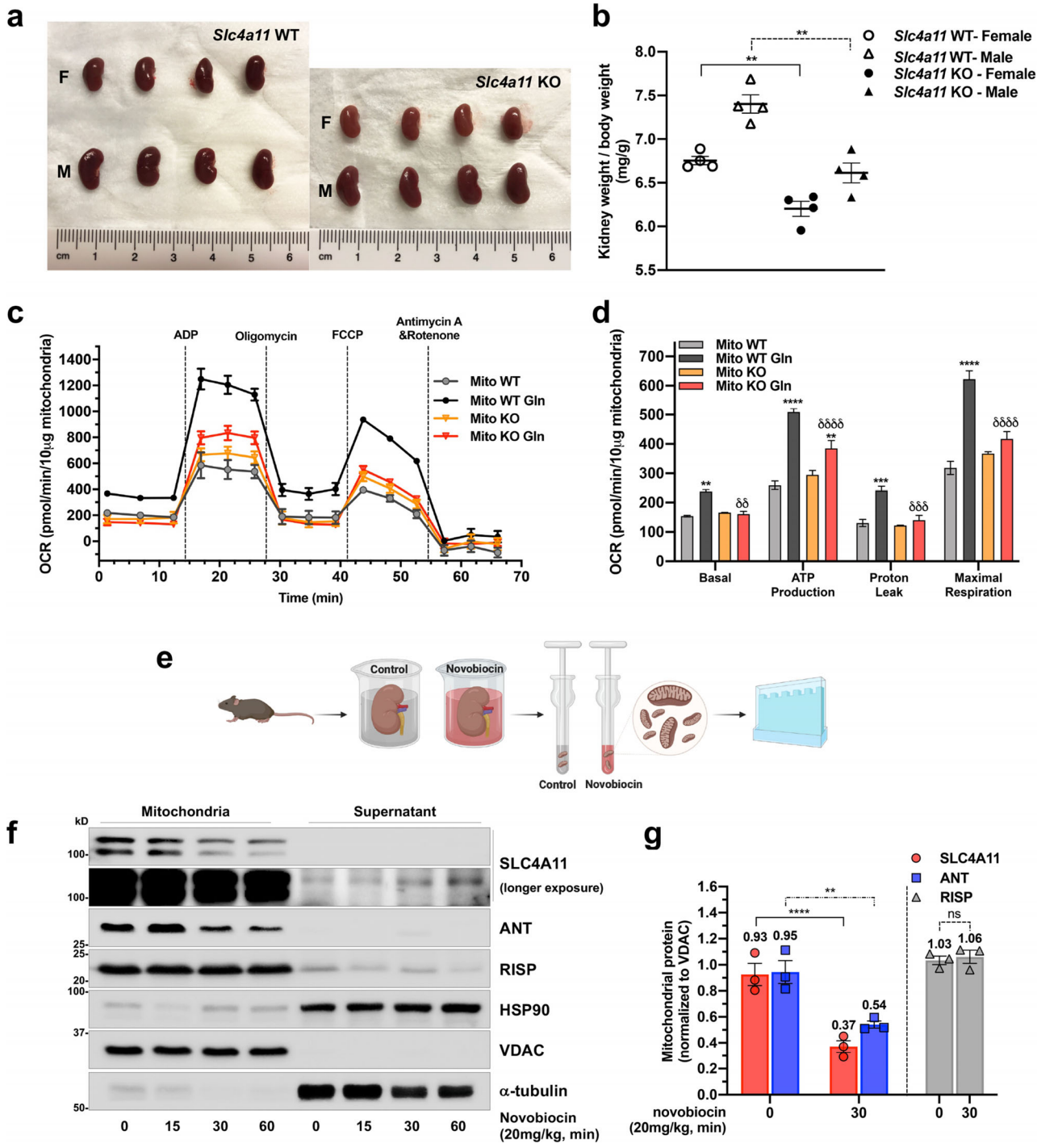

Figure 5. SLC4A11 presents in the mitochondria in the *Slc4a11* WT mice kidney. (**a**) Representative photo of 8-week-old kidney from *Slc4a11* WT and KO male and female mice. Size is shown in centimeters for scale. Kidneys were removed at termination and directly compared. $n = 4$ biologically independent mice per genotype and gender. (**b**) Graph comparing the ratio of kidney weight to body weight of *Slc4a11* WT and KO male and female mice shown in panel (**a**) and expressed as mg/g. Mean ± SEM. $n = 4$ biologically independent mice per genotype and gender. Significances were tested against the corresponding *Slc4a11* KO by a two-tailed Welch's *t*-test (**$P < 0.0021$, for same gender). (**c**) Mitochondrial OCR of kidney mitochondria from *Slc4a11* WT and KO mice was measured using a Seahorse XF Mito Stress Test. The mitochondria were purified from *Slc4a11* WT and KO kidneys ($n = 3$ biologically independent kidneys per genotype). (**d**) Summary of results from panel (**c**). Mean ± SEM. Significance levels were tested by a two-way ANOVA with Tukey's multiple comparison test from $n = 3$ (**$P < 0.0021$, ***$P < 0.0002$, and ****$P < 0.0001$ versus without Gln for same genotype; $\delta\delta P < 0.0021$, $\delta\delta\delta P < 0.0002$, and $\delta\delta\delta\delta P < 0.0001$ versus WT for same treatment). (**e**) Experimental procedure flowchart: the extent of mitochondrial Slc4a11 transport in the presence of HSP90 inhibitors was analyzed by immunoblotting mitochondrial and supernatant fractions from *Slc4a11* WT kidney after preconditioning with 20 mg/kg novobiocin for indicated times at 37°C. (**f**) Western blot of each fraction showing the effect of mitochondrial Slc4a11 translocation by HSP90 in *Slc4a11* WT kidney. (**g**) Quantification of Western blots of mitochondrial fraction from panel (**f**). Mean values ± SEM are present above the *bar*, and significance levels were tested by a two-way ANOVA with Bonferroni's multiple comparison. $n = 3$ biologically independent kidneys (**$P < 0.0021$, ****$P < 0.0001$, and ns = not significant).

Investigative Ophthalmology & Visual Science

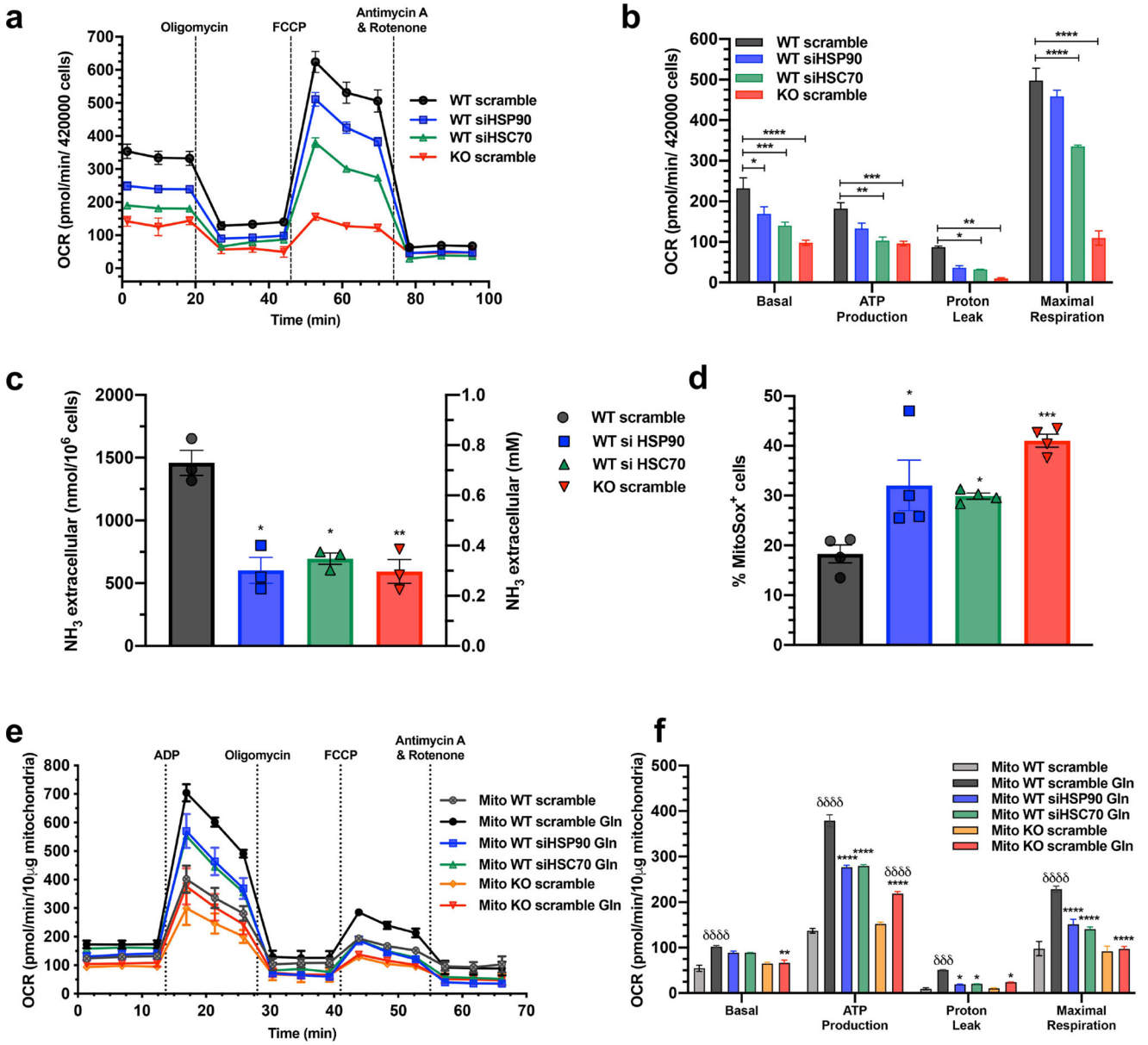

Figure 6. Failure in Slc4a11 translocation disrupts an NH_3-sensitive Slc4a11 mitochondrial uncoupling. (**a**) Mitochondrial OCR of WT MCECs after knockdown of HSP90 or HSC70 was determined using a Seahorse XFe24 Mito Stress Test. MCECs were preincubated in XF Base Medium supplemented with 1 g/L glucose and 0.5 mM Gln for 45 minutes in a non-CO_2 37°C incubator. OCR was measured three times each for baseline followed by injections of 2 µM oligomycin, 0.5 µM FCCP, and 0.5 µM rotenone and antimycin A, respectively. (**b**) Summary of results from (**a**). Mean ± SEM. $n = 4$. $^*P < 0.0332$, $^{**}P < 0.0021$, $^{***}P < 0.0002$, and $^{****}P < 0.0001$ versus WT scramble; two-way ANOVA with Tukey's multiple comparison test. (**c**) Ammonia production in DMEM assay media containing 1 g/L glucose, 0.5 mM Gln, and 0.5% dialyzed FBS that were incubated for 20 hours in WT and KO MCECs after 48 hours posttransfection with indicated siRNAs. Mean ± SEM. $n = 3$. $^*P < 0.0332$ and $^{**}P < 0.0021$; one-way ANOVA with a Dunnett's T3 multiple comparison test. (**d**) Flow cytometric analysis of mitochondrial ROS in WT and KO MCECs transfected with indicated siRNAs (see also Supplementary Fig. S4a). Mean ± SEM. $n = 3$. $^*P < 0.0332$ and $^{***}P < 0.0002$; one-way ANOVA with Dunnett's T3 multiple comparison test. (**e**, **f**) OCR trace and summary results of mitochondria purified from WT and KO MCECs after posttransfection with indicated siRNAs. In total, 10 µg mitochondria was preincubated in mitochondrial assay buffer containing 10 mM pyruvic acid, 2 mM malic acid, and ± 4 mM Gln. OCR was measured three times each for baseline following sequential injections of 2 mM ADP, 3 µM oligomycin, 4 µM FCCP, and 4 µM rotenone and antimycin A, respectively. Mean ± SEM. $n = 3$. $^*P < 0.0332$, $^{**}P < 0.0021$, and $^{****}P < 0.0001$ versus WT scramble Gln; $\delta\delta\delta P < 0.0002$ and $\delta\delta\delta\delta P < 0.0001$ versus without Gln for same genotype; two-way ANOVA with Tukey's multiple comparison test.

increased significantly more in WT. Moreover, calculated proton leak (Fig. 5d) was increased by Gln in WT but not KO, consistent with a previous study showing NH_3-sensitive mitochondrial uncoupling by Slc4a11.[14] Immunoblotting analysis of mitochondrial and supernatant fractions from *Slc4a11* WT kidneys (Fig. 5e) revealed that Slc4a11 was markedly enriched in mitochondria (Fig. 5f). To examine carrier-mediated targeting, kidneys were preconditioned with 20 mg/kg novobiocin, and mitochondrial and supernatant fractions were analyzed by immunoblotting. Figure 5f shows significant reduction of Slc4a11 and ANT but not RISP expression in the mitochondrial fraction with novobiocin

Investigative Ophthalmology & Visual Science

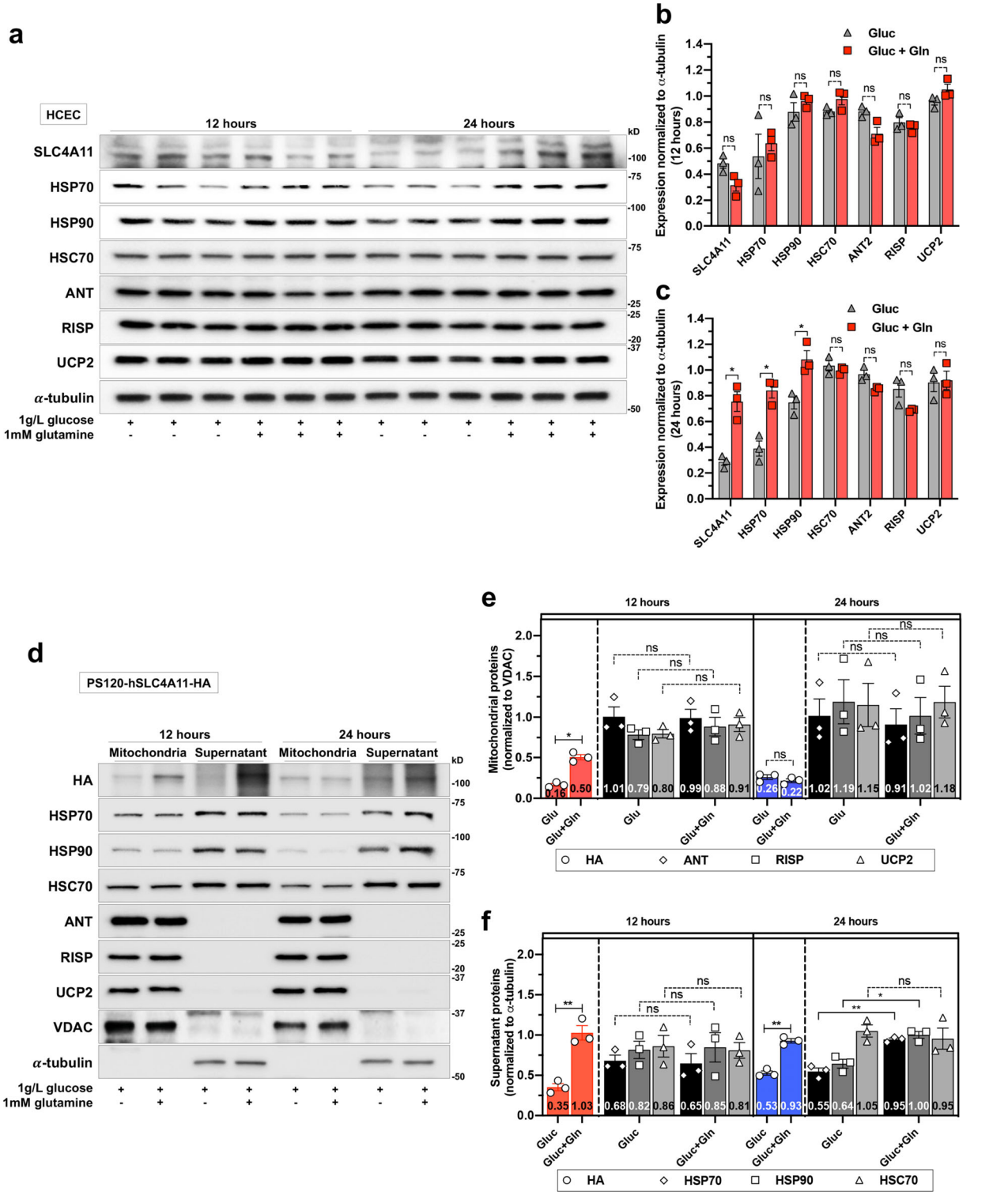

Figure 7. Glutamine induces the expression of SLC4A11 and HSPs. (**a**) Western blotting of SLC4A11 and HSPs in HCECs incubated with 1 mM glutamine (Gln) for 12 and 24 hours. Control group cells were incubated with glucose (Gluc) alone ($n = 3$ biologically independent samples per treatment). (**b**) Quantification of Western blots at 12 hours Gln treatment from panel (**a**). Mean values ± SEM. Significance tested against control group by a two-tailed *t*-test (ns = not significant). (**c**) Quantification of Western blots at 24 hours Gln treatment from panel (**a**). Mean values ± SEM. Significance tested against control group by a two-tailed *t*-test (*$P < 0.0332$ and ns = not significant). (**d**) Representative immunoblot of mitochondrial and supernatant fractions from PS120-hSLC4A11-HA cells that were treated with and without 1 mM Gln for 12 and 24 hours ($n = 3$ biologically independent samples per treatment). (**e**) Quantification of Western blots of mitochondrial fraction from (**d**) that were normalized relative to VDAC. Mean values ± SEM. Significance tested against the corresponding control group by a two-way ANOVA with Bonferroni's multiple comparison. (**f**) Quantification of Western blots of supernatant fraction from (**d**) that were normalized relative to α-tubulin. Mean values ± SEM. Significances tested against the corresponding control group by a two-way ANOVA with Bonferroni's multiple comparison.

Investigative Ophthalmology & Visual Science

treatment (Figs. 5f, 5g). In sum, our data show that Slc4a11 is present in kidney mitochondria and HSP90 is necessary for trafficking to the mitochondria. Furthermore, Slc4a11 in the kidneys facilitates Gln catabolism and provides mitochondrial uncoupling.

Chaperone Interference Inhibits Mitochondrial Slc4a11 Function in Corneal Endothelium

SLC4A11 facilitates Gln catabolism in CE by suppressing the damaging effects of an activated electron transport chain (ETC) and NH_3.[14] In particular, SLC4A11 limits mitochondrial ROS by functioning as an NH_3-sensitive uncoupler, which suppresses mitochondrial membrane potential (MMP) hyperpolarization in the IMM.[14] Since mitochondrial SLC4A11 import is mediated by chaperone-dependent trafficking, HSP90 or HSC70 knockdown should disrupt SLC4A11 mitochondrial function. We investigated the effects of siRNA against HSP90 or HSC70 in WT MCECs by measuring oxygen consumption (OCR) following the addition of specific inhibitors of the ETC. Figures 6a and 6b show that knockdown of HSC70 in WT MCECs resulted in significant reduction of glutamine-dependent oxygen utilization and reduction in proton leak (oligomycin – rotenone and antimycin A) and ATP-linked respiration when compared with WT MCECs. Similarly, HSP90 knockdown showed decreases of all OCR parameters, but only basal respiration was statistically significant (Figs. 6a, 6b). Consistent with reduced OCR, Gln consumption, measured by NH_3 production, in WT MCECs transfected with HSP90 or HSC70 siRNAs was significantly reduced relative to WT and similar to KO MCECs (Fig. 6c).

Mitochondrial ROS generated by an energized ETC during Gln catabolism and the direct action of Gln-derived NH_3 on the ETC damaged mitochondria in KO MCECs due to the absence of Slc4a11 uncoupling.[14] We observed that altered mitochondrial Slc4a11 import by knockdown of HSP90 and HSC70 in WT MCECs caused higher levels of mitochondrial ROS in response to Gln, similar to *Slc4a11* KO MCECs (Fig. 6d). These data indicate that failure of Slc4a11 trafficking to the IMM increases mitochondrial ROS production during glutamine catabolism.

Next, we used isolated mitochondria to avoid potential confounding variables from plasma membrane SLC4A11 and other sources of Gln-derived NH_3. Figure 6e shows OCR using mitochondria purified from WT and KO MCECs that had been transfected with HSC70 or HSP90 siRNAs with and without glutamine. All OCR parameters in response to Gln were significantly higher in WT mitochondria compared to KO mitochondria. Mitochondria from WT MCECs transfected with either HSP90 or HSC70 siRNA showed a significant reduction in all OCR parameters, specifically proton leak–linked respiration with exposure to Gln (Figs. 6e, 6f). The OCR analysis of isolated mitochondria provided confirmation that the altered cellular OCR characteristics due to HSP90 and HSC70 siRNA were not secondary to plasma membrane or other potential locations of SLC4A11.

Glutamine Upregulates SLC4A11, HSP70, and HSP90 Expression

Glutamine catabolism within mitochondria accelerates the ETC inducing increased ROS production,[14–17] and ROS is known to increase SLC4A11 expression via NRF2 activation.[50] Therefore, we examined the effect of Gln on SLC4A11 expression as well as cellular cytoprotective heat shock proteins (HSPs), which are induced by various of stress stimuli. Gln significantly increased inducible HSP70 and HSP90 α/β protein expression after 24 hours post-Gln treatment in both HCECs and PS120-hSLC4A11-HA cells, whereas constitutive HSC70 expression did not change. Interestingly, Gln upregulated the expression of SLC4A11 in both HCECs at 24 hours and in PS120-hSLC4A11-HA cells at 12 and 24 hours (Figs. 7a–c and Supplementary Figs. S5a, S5b). As the total expression of SLC4A11 was upregulated by Gln, we next asked whether the upregulated SLC4A11 affects the level of mitochondrial SLC4A11 under the same condition. A significant increase in SLC4A11 expression in the mitochondrial fraction was induced by Gln at 12 hours in both HCECs and PS120-hSLC4A11-HA cells. Induction of cytoplasmic HSP70 and HSP90 but not HSC70 expression were slightly increased at 12 hours and statistically significant at 24 hours. The expression of SLC4A11 in the supernatant fraction, including plasma membrane and cytoplasmic proteins, was also upregulated by Gln at 12 to 24 hours (Figs. 7d–f and Supplementary Figs. S5c, S5d). Taken together, these results indicate that increased oxidative stress caused by Gln catabolism not only induces HSP70 and HSP90 but also confers cell protection by upregulation of the expression of SLC4A11 and mitochondrial targeting.

Discussion

Our data support a model (Fig. 8) wherein SLC4A11 can traffic to mitochondria with the aid of HSC70 and HSP90—chaperone complexes that can be recruited to bind to the surface receptor, TOM70, thereby allowing SLC4A11 to traverse to the IMM, where it functions as an NH_3-sensitive mitochondrial uncoupler. Glutamine catabolism significantly increases ETC flux (i.e., increased OCR), providing a strong MMP hyperpolarizing force. If left unchecked (e.g., in Slc4a11 KO), a hyperpolarized mitochondria yields excessive ammonia-dependent ROS production that significantly damages mitochondria.[14] As such, functional consequences of interfering with mitochondrial SLC4A11 translocation included reduced Gln consumption, reduced Gln-dependent oxygen consumption and proton leak, and increased ROS, which is the *Slc4a11* KO phenotype.

Our previous study using CE cells and *SLC4A11*-transfected PS120 fibroblasts showed IMM localization of SLC4A11 and its function as an NH_3-activated mitochondrial uncoupler.[14] N-terminus analysis indicated a low probability of presequence mitochondrial targeting for SLC4A11. The predictors had minor discrepancies, but on the whole, they were in agreement. Our previous data[14] and this work clearly show that SLC4A11, as a newly discovered mitochondrial protein, is highly enriched in the IMM by traversing through a chaperone-mediated carrier pathway. The LC-MS/MS analysis identified molecular chaperones as putative interactors of SLC4A11 responsible for mitochondrial SLC4A11 import, suggesting that HSC70 and HSP90 were leading candidates. HSP90β is the constitutive isoform, whereas stress factor–derived HSP90α only appeared to be associated with SLC4A11 protein in the PS120-hSLC4A11-HA whole-cell lysates (Supplementary Fig. S1c). Detection of only HSP90β is likely due to the lower relative abundance of HSP90 proteins in the cytoplasm that may limit analytical detection in whole-cell fractions. Because HSP90 proteins account for only 1% to 2% of total cellular proteins under nonstress

Investigative Ophthalmology & Visual Science

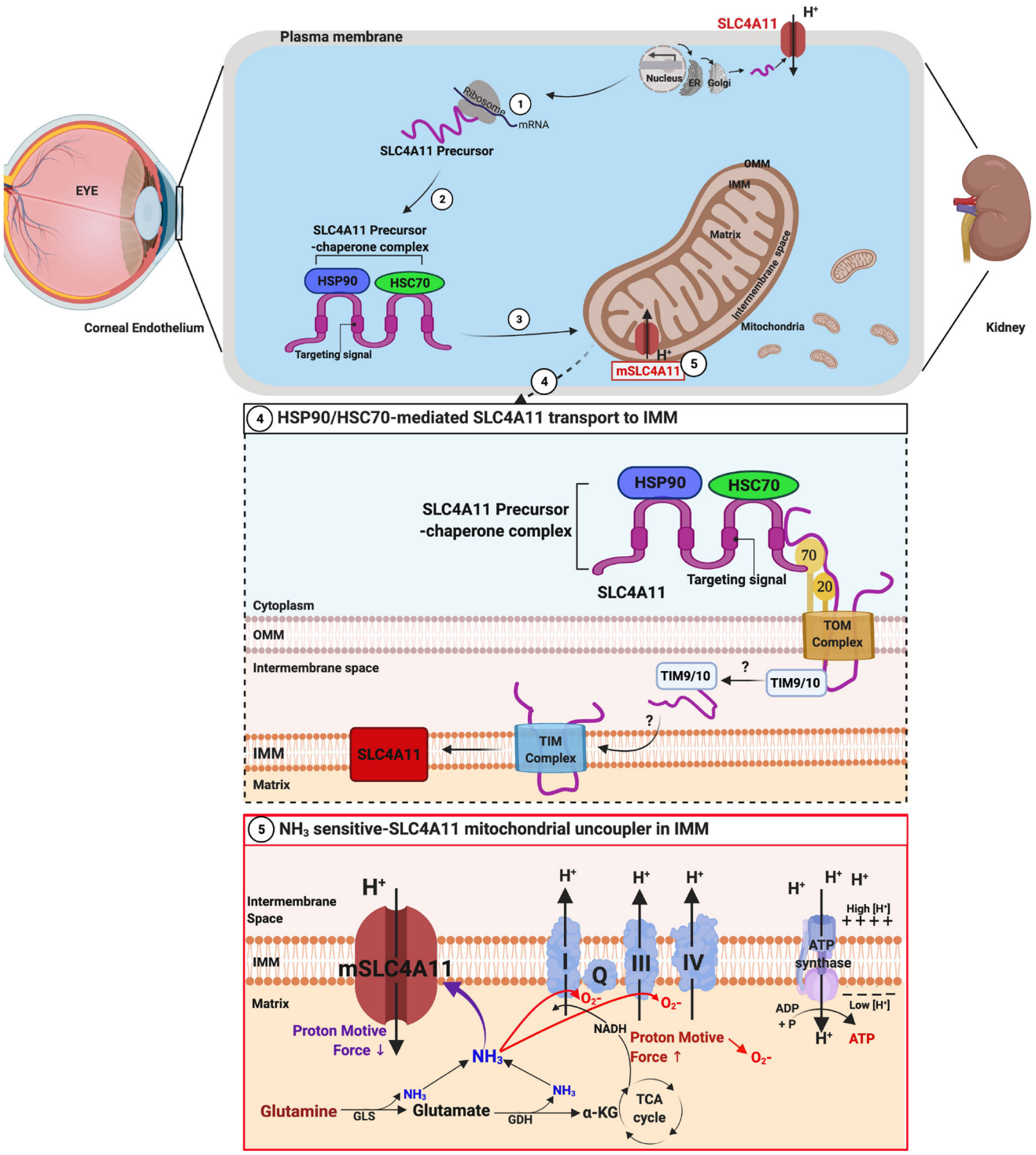

Figure 8. Schematic model for the chaperone-mediated carrier pathway in targeting mitochondrial SLC4A11. (1) The nuclear-encoded SLC4A11 precursors are synthesized on cytoplasmic or endoplasmic reticulum (ER)-bound ribosomes. (2) Chaperones, HSP90, and/or HSC70 in the cytosol bind to SLC4A11 precursors to prevent their aggregation, to escort them to the mitochondria, and to bind specifically to TOM70. (3) SLC4A11 precursor–chaperone (HSP90 and/or HSC70) complexes are targeted to the mitochondrial surface, specifically to TOM70. (4) After traversing across the OMM through the TOM complex, TIM9–TIM10 chaperones in the intermembrane space possibly transfer the SLC4A11 to the IMM. Finally, SLC4A11 is laterally released into the inner membrane of mitochondria, although the mechanism of release has not yet been clarified. (5) At the IMM, SLC4A11 acts as an ammonia-sensitive uncoupler that reduces MMP hyperpolarization, which suppresses ROS production during glutamine-induced electron transport chain activity, thereby protecting mitochondria.

Investigative Ophthalmology & Visual Science

conditions, HSP90β expression level is, in general, higher compared to HSP90α in most cells.[51]

With regard to the mechanism by which cytosolic molecular chaperones mediate the targeting of mitochondrial precursors to the mitochondrial surface receptor TOM70, there is extensive evidence linking involvement of HSP90, HSP70, and HSC70 in this pathway, known as the carrier pathway.[21,25] The mechanism of HSP90 action in the context of TOM70-dependent mitochondrial precursor trafficking has been demonstrated by using two HSP90 inhibitors that have different inhibitory mechanisms: (1) novobiocin targets the C-terminal domain of HSP90, causing degradation of the preprotein–chaperone complex in the cytosol, and (2) geldanamycin binds to the ADP/ATP binding pocket on the N-terminal domain of HSP90, inhibiting targeting of precursors to the outer mitochondrial membrane.[20,21,46,47] Consistent with this observation, both pharmacologic inhibitors of HSP90 reduced the mitochondrial SLC4A11 translocation, which parallels the disruption of mitochondrial SLC4A11 import by siRNA knockdown of the chaperones HSP90 and HSC70. What is less clear is whether the chaperones act together in trafficking SLC4A11 or can work alone. Moreover, transport of "carrier pathway"–dependent precursors in the intermembrane space to IMM is predominantly through TIM9–TIM10.[52,53] We suspect that TIM9–TIM10 may be at work in the intermembrane space to guide SLC4A11 into IMM, but further studies are needed.

A study by Gee et al.[54] showed the expression of Slc4a11 in the upper descending thin limbs of the mouse kidney, which was hypothesized as a transporter-modulating ammonia recycling in the outer medulla. Slc4a11 localization to kidney mitochondria and OCR analysis using isolated kidney mitochondria reveal similar characteristics of SLC4A11 as in corneal endothelium and transfected fibroblasts. While we postulate that Slc4a11 acts potentially as an NH_3-sensitive mitochondrial uncoupler in renal proximal tubule mitochondria where the majority of ammonia is produced by Gln catabolism, its specific expression profile over the kidney segments, submitochondrial localization, and transport kinetics in response to Gln requires further analysis.

SLC4A11 overexpression protects HCECs from oxidative stress. Oxidative stress induces SLC4A11 expression, which requires the transcription factor NRF2-mediated antioxidant signaling.[50] We show here that Gln catabolism, which induces oxidative stress, increases HSP70 and HSP90 and is in part cytoprotective by promoting mitochondrial targeting of the NH_3-sensitive uncoupler SLC4A11, providing attenuation of excessive hyperpolarization as a defense against mitochondrial oxidative stress. Slc4a11 confers mild mitochondrial uncoupling that could interconnect with other cellular mechanisms, including autophagy, mitophagy, Ca^+ homeostasis, and apoptosis.[55] Mitochondria are the source and targets of inevitable ROS by-products generated from an energized ETC and from the direct action of NH_3 on complexes I and III during Gln catabolism.[15–17] The cellular stress caused by continuous oxidative stress during Gln catabolism has been thought to be offset by increased production of glutathione and reduced NADP. This can be also curtailed by virtue of induction of SLC4A11, HSP70, and HSP90, which is consistent with previous reports of the role of SLC4A11 as an oxidative response gene.[50,56] However, further studies of the underlying mechanism of SLC4A11 in facilitating Gln catabolism in response to oxidative stress are needed. Moreover, further work should focus on those tissues (e.g., gut epithelium[57–59] and vascular endothelium[60]) that upregulate glutamine consumption during stress.

Last, to validate the targeting by these chaperones, we examined the metabolic consequences of blocking delivery of SLC4A11 to mitochondria. We found reduced mitochondrial SLC4A11 import (~ 60% between 68 and 70 hours), caused by inhibition of HSP90 and HSC70 in WT MCECs, resulted in lower levels of oxygen consumption and proton leak, a reduction of NH_3 production, and a significant increase in %MitoSOX$^+$ cells compared to the WT MCEC control. This change in cellular respiration and ROS levels in WT MCECs with chaperone disruption was similar to *Slc4a11* KO.[14] Importantly, OCR analysis of isolated mitochondria provided confirmation that the altered cellular characteristics were not secondary to plasma membrane or other potential locations of SLC4A11. Further research is required to understand whether any of the *SLC4A11* mutants implicated in human disease have specific defects in interactions with HSC70/HSP90 chaperones and mitochondrial targeting.

Acknowledgments

The authors thank Christiane Hassel, Indiana University Flow Cytometry Core Facility; Jonathan Trinidad and YiXing Zhang, Indiana University Biological Mass Spectrometry Facility; and Catherine Cheng for reviewing the manuscript, helpful suggestions on confocal experiments, image analysis, and use of Zeiss LSM 800 confocal microscope; and Chia-yang Liu for use of an EVOS FL Auto Imaging System.

Supported by NIH NEI/R01EY031321 and NIH NEI/R01EY008834 (JAB) and Sigma Xi Grant-in-Aid of Research (GIAR)/G20190315102187176 (MC).

Disclosure: **M. Choi**, None; **J.A. Bonanno**, None

References

1. Parker MD, Ourmozdi EP, Tanner MJ. Human BTR1, a new bicarbonate transporter superfamily member and human AE4 from kidney. *Biochem Biophys Res Commun*. 2001;282(5):1103–1109.
2. Vilas GL, Morgan PE, Loganathan SK, Quon A, Casey JR. A biochemical framework for SLC4A11, the plasma membrane protein defective in corneal dystrophies. *Biochemistry*. 2011;50(12):2157–2169.
3. Vilas GL, Loganathan SK, Quon A, Sundaresan P, Vithana EN, Casey J. Oligomerization of SLC4A11 protein and the severity of FECD and CHED2 corneal dystrophies caused by SLC4A11 mutations. *Hum Mutat*. 2012;33(2):419–428.
4. Zhang W, Ogando DG, Bonanno JA, Obukhov AG. Human SLC4A11 is a novel NH3/H+ co-transporter. *J Biol Chem*. 2015;290(27):16894–16905.
5. Kao L, Azimov R, Shao XM, et al. SLC4A11 function: evidence for H(+)(OH(-)) and NH3-H(+) transport. *Am J Physiol Cell Physiol*. 2020;318(2):C392–C405.
6. Park M, Li Q, Shcheynikov N, Zeng W, Muallem S. NaBC1 is a ubiquitous electrogenic Na+-coupled borate transporter essential for cellular boron homeostasis and cell growth and proliferation. *Mol Cell*. 2004;16(3):331–341.
7. Damkier HH, Nielsen S, Praetorius J. Molecular expression of SLC4-derived Na+-dependent anion transporters in selected human tissues. *Am J Physiol Regul Integr Comp Physiol*. 2007;293(5):R2136–R2146.
8. Jiao X, Sultana A, Garg P, Ramamurthy B, Vemuganti GK, Gangopadhyay N, et al. Autosomal recessive corneal

endothelial dystrophy (CHED2) is associated with mutations in SLC4A11. *J Med Genet*. 2007;44(1):64–68.

9. Siddiqui S, Zenteno JC, Rice A, et al. Congenital hereditary endothelial dystrophy caused by SLC4A11 mutations progresses to Harboyan syndrome. *Cornea*. 2014;33(3):247–251.
10. Han SB, Ang HP, Poh R, et al. Mice with a targeted disruption of Slc4a11 model the progressive corneal changes of congenital hereditary endothelial dystrophy. *Invest Ophthalmol Vis Sci*. 2013;54(9):6179–6189.
11. Groger N, Frohlich H, Maier H, et al. SLC4A11 prevents osmotic imbalance leading to corneal endothelial dystrophy, deafness, and polyuria. *J Biol Chem*. 2010;285(19):14467–14474.
12. Kao L, Azimov R, Shao XM, et al. Multifunctional ion transport properties of human SLC4A11: comparison of the SLC4A11-B and SLC4A11-C variants. *Am J Physiol Cell Physiol*. 2016;311(5):C820–C830.
13. Alka K, Casey JR. Ophthalmic nonsteroidal anti-inflammatory drugs as a therapy for corneal dystrophies caused by SLC4A11 mutation. *Invest Ophthalmol Vis Sci*. 2018;59(10):4258–4267.
14. Ogando DG, Choi M, Shyam R, Li S, Bonanno JA. Ammonia sensitive SLC4A11 mitochondrial uncoupling reduces glutamine induced oxidative stress. *Redox Biol*. 2019;26:101260.
15. Davuluri G, Allawy A, Thapaliya S, et al. Hyperammonaemia-induced skeletal muscle mitochondrial dysfunction results in cataplerosis and oxidative stress. *J Physiol*. 2016;594(24):7341–7360.
16. Jayakumar AR, Rama Rao KV, Schousboe A, Norenberg MD. Glutamine-induced free radical production in cultured astrocytes. *Glia*. 2004;46(3):296–301.
17. Grivennikova VG, Cecchini G, Vinogradov AD. Ammonium-dependent hydrogen peroxide production by mitochondria. *FEBS Lett*. 2008;582(18):2719–2724.
18. Jalimarada SS, Ogando DG, Vithana EN, Bonanno JA. Ion transport function of SLC4A11 in corneal endothelium. *Invest Ophthalmol Vis Sci*. 2013;54(6):4330–4340.
19. Schmidt O, Pfanner N, Meisinger C. Mitochondrial protein import: from proteomics to functional mechanisms. *Nat Rev Mol Cell Biol*. 2010;11(9):655–667.
20. Fan AC, Bhangoo MK, Young JC. Hsp90 functions in the targeting and outer membrane translocation steps of Tom70-mediated mitochondrial import. *J Biol Chem*. 2006;281(44):33313–33324.
21. Young JC, Hoogenraad NJ, Hartl FU. Molecular chaperones Hsp90 and Hsp70 deliver preproteins to the mitochondrial import receptor Tom70. *Cell*. 2003;112(1):41–50.
22. Wiedemann N, Truscott KN, Pfannschmidt S, Guiard B, Meisinger C, Pfanner N. Biogenesis of the protein import channel Tom40 of the mitochondrial outer membrane: intermembrane space components are involved in an early stage of the assembly pathway. *J Biol Chem*. 2004;279(18):18188–18194.
23. Li J, Qian X, Hu J, Sha B. Molecular chaperone Hsp70/Hsp90 prepares the mitochondrial outer membrane translocon receptor Tom71 for preprotein loading. *J Biol Chem*. 2009;284(35):23852–23859.
24. Zara V, Ferramosca A, Robitaille-Foucher P, Palmieri F, Young JC. Mitochondrial carrier protein biogenesis: role of the chaperones Hsc70 and Hsp90. *Biochem J*. 2009;419(2):369–375.
25. Rampelt H, Sucec I, Bersch B, et al. The mitochondrial carrier pathway transports non-canonical substrates with an odd number of transmembrane segments. *BMC Biol*. 2020;18(1):2.
26. Zhang W, Ogando DG, Kim ET, et al. Conditionally immortal Slc4a11–/– mouse corneal endothelial cell line recapitulates disrupted glutaminolysis seen in Slc4a11–/– mouse model. *Invest Ophthalmol Vis Sci*. 2017;58(9):3723–3731.
27. Schmedt T, Chen Y, Nguyen TT, Li S, Bonanno JA, Jurkunas UV. Telomerase immortalization of human corneal endothelial cells yields functional hexagonal monolayers. *PLoS One*. 2012;7(12):e51427.
28. Claros MG. MitoProt, a Macintosh application for studying mitochondrial proteins. *Comput Appl Biosci*. 1995;11(4):441–447.
29. Claros MG, Vincens P. Computational method to predict mitochondrially imported proteins and their targeting sequences. *Eur J Biochem*. 1996;241(3):779–786.
30. Emanuelsson O, Nielsen H, Brunak S, von Heijne G. Predicting subcellular localization of proteins based on their N-terminal amino acid sequence. *J Mol Biol*. 2000;300(4):1005–1016.
31. Bannai H, Tamada Y, Maruyama O, Nakai K, Miyano S. Extensive feature detection of N-terminal protein sorting signals. *Bioinformatics*. 2002;18(2):298–305.
32. Small I, Peeters N, Legeai F, Lurin C. Predotar: a tool for rapidly screening proteomes for N-terminal targeting sequences. *Proteomics*. 2004;4(6):1581–1590.
33. Ogando DG, Jalimarada SS, Zhang W, Vithana EN, Bonanno JA. SLC4A11 is an EIPA-sensitive Na(+) permeable pHi regulator. *Am J Physiol Cell Physiol*. 2013;305(7):C716–C727.
34. Schwer B, North BJ, Frye RA, Ott M, Verdin E. The human silent information regulator (Sir)2 homologue hSIRT3 is a mitochondrial nicotinamide adenine dinucleotide-dependent deacetylase. *J Cell Biol*. 2002;158(4):647–657.
35. Weisiger RA, Fridovich I. Mitochondrial superoxide simutase. Site of synthesis and intramitochondrial localization. *J Biol Chem*. 1973;248(13):4793–4796.
36. Gupta RS. Evolution of the chaperonin families (Hsp60, Hsp10 and Tcp-1) of proteins and the origin of eukaryotic cells. *Mol Microbiol*. 1995;15(1):1–11.
37. Holcomb T, Taylor L, Trohkimoinen J, Curthoys NP. Isolation, characterization and expression of a human brain mitochondrial glutaminase cDNA. *Brain Res Mol Brain Res*. 2000;76(1):56–63.
38. Sollner T, Griffiths G, Pfaller R, Pfanner N, Neupert W. MOM19, an import receptor for mitochondrial precursor proteins. *Cell*. 1989;59(6):1061–1070.
39. Mattiazzi M, D'Aurelio M, Gajewski CD, et al. Mutated human SOD1 causes dysfunction of oxidative phosphorylation in mitochondria of transgenic mice. *J Biol Chem*. 2002;277(33):29626–29633.
40. Bijur GN, Jope RS. Rapid accumulation of Akt in mitochondria following phosphatidylinositol 3-kinase activation. *J Neurochem*. 2003;87(6):1427–1435.
41. Aquilano K, Vigilanza P, Baldelli S, Pagliei B, Rotilio G, Ciriolo MR. Peroxisome proliferator-activated receptor gamma co-activator 1alpha (PGC-1alpha) and sirtuin 1 (SIRT1) reside in mitochondria: possible direct function in mitochondrial biogenesis. *J Biol Chem*. 2010;285(28):21590–21599.
42. Endres M, Neupert W, Brunner M. Transport of the ADP/ATP carrier of mitochondria from the TOM complex to the TIM22.54 complex. *EMBO J*. 1999;18(12):3214–3221.
43. Giardina TM, Steer JH, Lo SZ, DA Joyce. Uncoupling protein-2 accumulates rapidly in the inner mitochondrial membrane during mitochondrial reactive oxygen stress in macrophages. *Biochim Biophys Acta*. 2008;1777(2):118–129.
44. Soderberg O, Gullberg M, Jarvius M, et al. Direct observation of individual endogenous protein complexes in situ by proximity ligation. *Nat Methods*. 2006;3(12):995–1000.
45. Fredriksson S, Gullberg M, Jarvius J, et al. Protein detection using proximity-dependent DNA ligation assays. *Nat Biotechnol*. 2002;20(5):473–477.

Investigative Ophthalmology & Visual Science

46. Rodriguez-Sinovas A, Boengler K, Cabestrero A, et al. Translocation of connexin 43 to the inner mitochondrial membrane of cardiomyocytes through the heat shock protein 90-dependent TOM pathway and its importance for cardioprotection. *Circ Res*. 2006;99(1):93–101.
47. Budas GR, Churchill EN, Disatnik MH, Sun L, Mochly-Rosen D. Mitochondrial import of PKCepsilon is mediated by HSP90: a role in cardioprotection from ischaemia and reperfusion injury. *Cardiovasc Res*. 2010;88(1):83–92.
48. Barksdale KA, Bijur GN. The basal flux of Akt in the mitochondria is mediated by heat shock protein 90. *J Neurochem*. 2009;108(5):1289–1299.
49. Hall AM, Unwin RJ. The not so 'mighty chondrion': emergence of renal diseases due to mitochondrial dysfunction. *Nephron Physiol*. 2007;105(1):p1–p10.
50. Guha S, Chaurasia S, Ramachandran C, Roy S. SLC4A11 depletion impairs NRF2 mediated antioxidant signaling and increases reactive oxygen species in human corneal endothelial cells during oxidative stress. *Sci Rep*. 2017;7(1):4074.
51. Sreedhar AS, Kalmar E, Csermely P, Shen YF. Hsp90 isoforms: functions, expression and clinical importance. *FEBS Lett*. 2004;562(1–3):11–15.
52. Koehler CM. New developments in mitochondrial assembly. *Annu Rev Cell Dev Biol*. 2004;20:309–335.
53. Neupert W, Herrmann JM. Translocation of proteins into mitochondria. *Annu Rev Biochem*. 2007;76:723–749.
54. Gee MT, Kurtz I, Pannabecker TL. Expression of SLC4A11 protein in mouse and rat medulla: a candidate transporter involved in outer medullary ammonia recycling. *Physiol Rep*. 2019;7(10):e14089.
55. Demine S, Renard P, Arnould T. Mitochondrial uncoupling: a key controller of biological processes in physiology and diseases. *Cells*. 2019;8(8):795.
56. Roy S, Praneetha DC, Vendra VP. Mutations in the corneal endothelial dystrophy-associated gene SLC4A11 render the cells more vulnerable to oxidative insults. *Cornea*. 2015;34(6):668–674.
57. Ehrenfried JA, Chen J, Li J, Evers BM. Glutamine-mediated regulation of heat shock protein expression in intestinal cells. *Surgery*. 1995;118(2):352–356; discussion 6–7.
58. Noguchi Y, James JH, Fischer JE, Hasselgren PO. Increased glutamine consumption in small intestine epithelial cells during sepsis in rats. *Am J Surg*. 1997;173(3):199–205.
59. Tapiero H, Mathe G, Couvreur P, Tew KD, II. Glutamine and glutamate. *Biomed Pharmacother*. 2002;56(9):446–457.
60. Unterluggauer H, Mazurek S, Lener B, et al. Premature senescence of human endothelial cells induced by inhibition of glutaminase. *Biogerontology*. 2008;9(4):247–259.

Investigative Ophthalmology & Visual Science